Can Nonlinear Hydromagnetic Waves Support a Self-Gravitating Cloud?

Charles F. Gammie and Eve C. Ostriker
Harvard-Smithsonian Center for Astrophysics, MS-51
60 Garden St., Cambridge, MA 02138

ABSTRACT

Using self-consistent magnetohydrodynamic (MHD) simulations, we explore the hypothesis that nonlinear MHD waves dominate the internal dynamics of galactic molecular clouds. Our models employ an isothermal equation of state and allow for self-gravity. We adopt "slab-symmetry," which permits motions $\mathbf{v}_\perp$ and fields $\mathbf{B}_\perp$ perpendicular to the mean field, but permits gradients only parallel to the mean field. This is the simplest possible geometry that relies on waves to inhibit gravitational collapse along the mean field. In our simulations, the Alfvén speed $v_{\rm A}$ exceeds the sound speed $c_{\rm s}$ by a factor $3-30$, which is realistic for molecular clouds. We simulate the free decay of a spectrum of Alfvén waves, with and without self-gravity. We also perform simulations with and without self-gravity that include small-scale stochastic forcing, meant to model the mechanical energy input from stellar outflows.

Our major results are as follows: (1) We confirm that the pressure associated with fluctuating transverse fields can inhibit the mean-field collapse of clouds that are unstable by Jeans's criterion. Cloud support requires the energy in Alfvén -like disturbances to remain comparable to the cloud's gravitational binding energy. (2) We characterize the turbulent energy spectrum and density structure in magnetically-dominated clouds. The perturbed magnetic and transverse kinetic energies are nearly in equipartition and far exceed the longitudinal kinetic energy. The turbulent spectrum evolves to a power-law shape, approximately $v_{\perp,k}^2 \approx B_{\perp,k}^2/4\pi\rho \propto k^{-s}$ with $s \sim 2$, i.e. approximately consistent with a "linewidth-size" relation $\sigma_v(R) \propto R^{1/2}$. The simulations show large density contrasts, with high density regions confined in part by the pressure of the fluctuating magnetic field. (3) We evaluate the input power required to offset dissipation through shocks, as a function of $c_{\rm s}/v_{\rm A}$, the velocity dispersion σ_v, and the characteristic scale λ of the forcing. In equilibrium, the volume dissipation rate is $5.5(c_{\rm s}/v_{\rm A})^{1/2}(\lambda/L)^{-1/2} \times \rho\sigma_v^3/L$, for a cloud of linear size L and density ρ. (4) Somewhat speculatively, we apply our results to a "typical" molecular cloud. The mechanical power input required for equilibrium

(tens of $L_\odot$), and the implied star formation efficiency ($\sim 1\%$), are in rough agreement with observations. Because this study is limited to slab symmetry and excludes ion-neutral friction, the dissipation rate we calculate probably provides a lower limit on the true value.

1. Introduction

The internal dynamics of star-forming galactic molecular clouds is not yet understood. Two central questions are (1) what prevents the clouds and their subcomponents from collapsing under their own weight; and (2) what generates and controls the turbulent fluid velocities that broaden molecular lines far beyond the thermal speed c_s (e.g. Shu et al. (1987)). One model which has been proposed (e. g. Scalo & Pumphrey (1982)) is that the clouds are comprised of clumps on essentially ballistic, collisionless orbits. However, while clouds are observed to be clumpy, the volume filling factor of clumps in the clouds $f \sim 0.03 - 0.08$ (e.g. Pérault, Falgarone, & Puget (1985); Williams, Blitz, & Stark (1995)) implies a clump-clump collision time $t_{\rm collis} < (4/3)R_{\rm clump}/(f v_{\rm clump}) \sim 10^7$yr, which makes the clouds at most marginally collisionless over their lifetimes (Blitz & Shu (1980)). The clumps are not themselves thermally supported, and they appear to have larger internal filling factors and smaller ratios of internal collision time to dynamical time. Although internal velocities may be generated by a cloud's self-gravity, purely hydrodynamic turbulence – either clumpy or smooth – cannot in itself support a structure for longer than the effective collision time (equal to the eddy-turnover time for a uniform fluid) because it would dissipate in shocks (see Elmegreen (1985) and references therein). The orbiting-clump model therefore probably cannot account for the internal dynamics of molecular clouds at all scales. [1] Rather than assuming a clumpy mass distribution *a priori*, it seems better to start with a full fluid model with a compressible equation of state, so that clumping can be treated self-consistently. Such a model must have some internal stress far more powerful than gas pressure in order to control supersonic motions.

For some time, magnetic fields have been considered the leading candidate for mediating clouds' internal motions and counteracting gravity (see the recent reviews of Shu et al. (1987); McKee et al. (1993)). Magnetic processes have also been identified as likely instruments for generating density structure within clouds (e.g. Elmegreen (1990); Elmegreen (1991)), which is observed at all scales down to the limiting telescopic resolution

[1] In particular, it is not apparent how a collisionless system could generate non-self-gravitating clumps whose internal velocity dispersions scale with their size (cf. Bertoldi & McKee (1992)).

(Falgarone, Phillips, & Walker (1991); Falgarone, Puget, & Pérault (1992)). Measured field strengths $B_{\|}$ based on OH Zeeman splittings are in the range $10 - 30\mu$G (Crutcher et al (1993)) for the line-of-sight field in moderate-density regions $n_{H_2} \gtrsim 1000\mathrm{cm}^{-3}$ (for random orientations the mean total field strength is twice as large). Fits incorporating additional data from weak-field, low-density HI Zeeman splitting and strong-field, high-density OH maser Zeeman splitting yield $B \approx 1.5(n_{H_2}/1\mathrm{cm}^{-3})^{1/2}\mu$G (Heiles et al. (1993), and references therein). Based on these data, the magnetic field has an energy density comparable to the kinetic (and gravitational) energy densities, and therefore can be dynamically important. More specifically, Myers & Goodman (1988a) show that magnetic, kinetic, and gravitational energies are comparable in detail for several clouds at a range of scales, suggesting virial equilibrium. The field topology within molecular clouds remains uncertain. In optical wavelengths, the linear polarization directions of background stars shining through low-density regions undulate smoothly across cloud complexes (e.g. Moneti et al (1984)). To trace higher-density gas within clouds, longer wavelengths are needed. Maps of polarized 100μ thermal emission in several high-mass star-forming regions ((Dotson (1995)), Hildebrand et al (1995), Davidson et al (1995)) also show orderly variation across the cloud. If in both cases the polarization is caused by field-aligned dust grains, the data imply smoothly-varying mean fields. These preliminary indications on field geometry, if confirmed, permit a conceptual separation into cloud support perpendicular to, and parallel to, a slowly-varying, untangled, mean field.

To date, most theoretical work on magnetic fields in star-forming regions has concentrated on the role of smooth fields in quasi-static equilibria or configurations undergoing laminar rotation and/or collapse (see the reviews of Nakano (1984); Mouschovias (1991); McKee et al. (1993)). The absence of turbulent velocities v_{turb} exceeding c_{s} in the small, dense cloud cores observed to be the sites of low-mass star formation (see, e.g. Fuller & Myers (1992)) makes them amenable to quasistatic theories. To the extent that turbulent magnetic and Reynolds stresses can be included via a barotropic pressure, such calculations can also be applied to cases where $v_{\mathrm{turb}} > c_{\mathrm{s}}$. Axisymmetric calculations of field-frozen equilibria have quantified the importance of field support perpendicular to the mean field direction, which can be expressed succinctly in terms of the mass-to-magnetic flux ratio, M/Φ (Mouschovias (1976a); Mouschovias & Spitzer (1976); Tomisaka, Ikeuchi, & Nakamura (1988)). The value of this evolutionary invariant determines whether or not an equilibrium can be sustained.

While static or time-averaged fields are likely key to cloud support at both small and large scales, they do not oppose gravity in the mean field direction, and by definition cannot produce a large velocity dispersion. For clumps within clouds (reviewed by Blitz (1993); see also Bertoldi & McKee (1992)), and massive cloud cores (e.g. Caselli & Myers

(1995)), however, molecular line observations exhibit linewidths in excess of $c_{\rm s}$. The inferred hypersonic bulk velocities were attributed to MHD waves shortly after their discovery (Arons & Max (1975)). For Alfvén waves, the fluctuating component of the field provides a pressure that acts along the mean field, and can therefore oppose gravity in that direction (Dewar (1970) ; Shu et al. (1987); Fatuzzo & Adams (1993); McKee & Zweibel (1995)).

The theory of Dewar (1970) calculates the influence of small-amplitude MHD waves on the background state of the fluid, using a locally-averaged Lagrangian. For Alfvén waves, the effect of the waves is expressed through an isotropic wave pressure $P_{\rm wave} = \langle|\delta\mathbf{B}|^2\rangle/8\pi$, where the magnetic disturbance is $\delta\mathbf{B}$. Recently, McKee & Zweibel (1995) have used Dewar's theory to show that small-amplitude Alfvén waves propagating along a density gradient obey $P_{\rm wave} \propto \rho^{1/2}$ (implying effective polytropic index $\gamma_p = 1/2$), while waves trapped in a contracting cloud obey $P_{\rm wave} \propto \rho^{3/2}$ (implying effective adiabatic index $\gamma_a = 3/2$). Since gas spheres are dynamically stable to adiabatic perturbations when $\gamma_a > 4/3$ (e.g. Cox (1980)), large amplitude Alfvén waves could potentially support a cloud against collapse if they suffered minimal decay, or loss (cf. Elmegreen (1985)) into the surrounding medium, and obeyed the same scaling. A crucial unknown is the decay rate of arbitrary amplitude MHD waves in conditions appropriate for a molecular cloud. If Alfvén waves are responsible for the internal linewidths of molecular clouds and support against gravity and external pressure, then any decay must be replenished if a quasi-equilibrium is to be maintained. Prior to high-mass star formation, the ultimate source of new wave energy must be the gravitational potential of the cloud (cf. Mestel & Spitzer (1956); Norman & Silk (1980); Falgarone & Puget (1986); McKee (1989)). Potential energy is liberated by overall cloud contraction and/or star formation (with winds); for quasi-equilibrium the respective rates would depend on how fast waves decay. At present, estimates of decay rates rely on analytic calculations of linear damping by ion-neutral friction, nonlinear single-wave steepening (see Zweibel & Josafatsson (1983) and references therein), or simply dimensional analysis in terms of the internal velocity dispersion and size (see Black (1987) and references therein).

Previous theoretical studies of MHD waves in molecular clouds have concentrated on the linear, adiabatic, WKB limit in analyzing wave dynamics (Fatuzzo & Adams (1993); McKee & Zweibel (1995); Zweibel & McKee (1995)). This approach is accurate when the amplitude of the wave is small, when the wavelength of the waves is much smaller than the size of the system, and when the wave damping is weak. Since the first two of these assumptions do not strictly apply in molecular clouds, and the third may not either, it is interesting to see if we can relax them somewhat. In this paper, we undertake to study the full nonlinear development of moderate-amplitude MHD disturbances in a self-gravitating system, using numerical simulations. We concentrate our attention on the most basic

questions of how well clouds can be supported against gravity by nonlinear disturbances, and how long it takes MHD turbulence to decay. By employing simulations, we can generalize ideas of support by simple Alfvén waves to include arbitrary self-consistent disturbances in the magnetic field, fluid flow, and density structure. We can test how far the linear-theory predictions for wave support carry over to the nonlinear regime, and go beyond the purview of simple linear theory to investigate the growth of structure, cascade of energy between scales, and associated dissipation.

Expedience demands some sacrifices of realism for this first study. Our most severe simplification is to restrict the motions to plane-parallel geometry, so all dynamical variables are functions of one independent space variable and time. Thus we allow for transverse motions but not transverse derivatives. Another idealization which is less serious for the large-scale motions we consider is the neglect of ambipolar diffusion. We shall also assume the gas is isothermal.

The plan of this paper is as follows. In §2 we review basic observational results for molecular clouds and the implied timescales in the context of simple theoretical considerations of cloud stability. We then present the equations we shall solve, our numerical method, and various tests used to verify its performance (§3). In §4 we describe the series of simulations we have performed. Finally, we apply our results to astronomical systems, discuss directions for future research, and summarize our conclusions (§5).

2. Summary of Observations and Theory

2.1. Cloud Properties and Scalings

At present, the overall dynamical characterization of molecular clouds (e.g. delayed collapse, quasistatic contracting or expanding equilibrium) remains uncertain. In particular, the uncertainties about formation mechanisms and difficulty of assigning ages hampers efforts to deduce evolutionary trends (e.g. Elmegreen (1993)). Arguments about the dynamical state are therefore indirect. The presence of several-million-year-old stars within cloud complexes indicates they have survived long enough to exceed the characteristic gravitational collapse times of at least the (higher-density) clumps; yet, a general internal collapse has not occurred. While cloud complex ages may not exceed the collapse times at their (lower) mean density, they are likely stabilized by something stronger than gas pressure because wholesale collapse on the dynamical times would lead to an unacceptably large galactic star formation rate (see review of Shu et al. (1987)). Indeed, the presence of substructure at all scales within molecular clouds reveals that something much more

interesting than a nearly-pressure-free collapse is taking place.

Spectral observations of molecular transitions show hypersonic widths everywhere except in the densest regions. These broad, often non-Gaussian molecular lines (Falgarone & Phillips (1990); Miesch & Scalo (1995)), give evidence that the gas they trace is in a highly turbulent state, with the turbulent amplitudes dependent on spatial scale. For cloud complexes, and massive component clumps and cores within them, internal linewidths σ_v typically increase with size scale R as $\sigma_v(R) \propto R^{1/2}$ (this type of scaling was first pointed out by Larson (1981); see also Dame et al (1986), Solomon et al (1987), Falgarone & Pérault (1987), Myers & Goodman (1988b)). Together with the typical observed scaling of mean density with size as $n \propto R^{-1}$ (Larson (1981)), this relation implies that internal velocities within these structures are roughly virial, consistent with a response to self-gravitational confinement. The internal kinetic energy densities in the lower-mass, non-self-gravitating clumps (e.g. Carr (1987), Loren (1989a), Loren (1989b), Herbertz, Ungerechts, & Winnewisser (1991), Falgarone, Puget, & Pérault (1992), Williams, Blitz, & Stark (1995)) are instead comparable to the mean internal energy density of the surrounding GMC, suggesting a balance of stresses at the interface between the clump and an interclump medium – "pressure confinement" (Bertoldi & McKee (1992)). The internal velocity and density structure in clouds points to the importance of magnetic fields; however, the lack of detailed information on field strengths and topology makes it difficult to decide how close to equilibrium any cloud, component clump, or core really is (see Goodman & Heiles (1994)). Below we outline cloud observed properties, define relevant timescales necessary for scaling our numerical simulations, and discuss the corresponding simple stability requirements assuming uniform conditions.

The average linear dimension L is typically 40pc for GMCs, 10pc for dark cloud complexes, and up to a few pc for the component clumps within these complexes that contain most of the mass. The volume-averaged density $n_{\rm H_2}$ is typically $25 - 100{\rm cm}^{-3}$ in cloud complexes, and $10^3{\rm cm}^{-3}$ in clumps. Kinetic temperatures range from $10 - 50{\rm K}$. This implies an isothermal sound speed $c_s = \sqrt{kT/\mu} = 0.19 - 0.41{\rm km\,s}^{-1}$, where $\mu = 2.4 m_p$ (e.g. Blitz (1993); Cernicharo (1991)). A convenient measure of the importance of magnetic fields is the parameter β, [2] defined by

$$\beta \equiv \frac{c_s^2}{v_A^2} = \frac{c_s^2}{B^2/4\pi\rho} = 0.021 \left(\frac{T}{10{\rm K}}\right) \left(\frac{n_{H_2}}{10^2{\rm cm}^{-3}}\right) \left(\frac{B}{10\mu{\rm G}}\right)^{-2}. \qquad (1)$$

$\beta < 1$ implies a magnetically-dominated regime. Generally β ranges between 0.1 and 0.001 in molecular clouds, reaching unity only in cloud cores. Notice that under isothermal,

[2]Our β differs by a factor of 2 from the usual plasma $\beta_p \equiv (gas\ pressure)/(magnetic\ pressure)$.

field-freezing conditions, β decreases as a cloud contracts homologously ($B \propto n^{2/3}$). It is therefore natural to expect the importance of magnetic forces to increase relative to gas pressure gradients as an efficiently-radiating cloud condenses out of the interstellar medium.

The sound wave crossing time over a scale L is

$$t_{\rm s} = \frac{L}{c_s} = 53 \left(\frac{L}{10{\rm pc}}\right) \left(\frac{T}{10{\rm K}}\right)^{-1/2} {\rm Myr}, \tag{2}$$

a characteristic gravitational collapse time is

$$t_{\rm c} = \left(\frac{\pi}{G\rho}\right)^{1/2} = 9.9 \left(\frac{n_{H_2}}{10^2{\rm cm}^{-3}}\right)^{-1/2} {\rm Myr}, \tag{3}$$

and the Alfvén wave crossing time over a distance L along a uniform field B_0 is

$$t_{\rm A} = \frac{L}{v_A} \equiv \frac{L\sqrt{4\pi\bar{\rho}}}{B_0)} = 7.6 \left(\frac{L}{10{\rm pc}}\right) \left(\frac{n_{H_2}}{10^2{\rm cm}^{-3}}\right)^{1/2} \left(\frac{B_0}{10\mu{\rm G}}\right)^{-1} {\rm Myr}. \tag{4}$$

2.2. Stability Requirements in a Uniform Medium

With the definition of collapse time in equation (3), the ratio of structure scale L to the Jeans length $L_{\rm J} \equiv c_{\rm s}(\pi/G\rho)^{1/2}$ satisfies $L/L_{\rm J} = t_{\rm s}/t_{\rm c}$, so structures with $t_{\rm s} > t_{\rm c}$ are above the Jeans limit and cannot be supported by thermal pressure alone. The importance of a mean field $\mathbf{B}_0$ to cloud dynamics can be measured by comparing the Alfvén crossing time $t_{\rm A} = L/v_{\rm A}$ to the characteristic collapse time $t_{\rm c}$,

$$\frac{t_{\rm A}}{t_{\rm c}} = 0.76 \left(\frac{L}{10{\rm pc}}\right) \left(\frac{n_{H_2}}{10^2{\rm cm}^{-3}}\right) \left(\frac{B_0}{10\mu{\rm G}}\right)^{-1}, \tag{5}$$

assuming a uniform field strength and density. When perturbations of wavelength L are applied to a cold medium with the wavevector perpendicular to the field, an analysis analogous to the classical Jeans treatment (Chandrasekhar & Fermi (1953)) shows that for $\beta \ll 1$ the perturbation is stable when $t_{\rm A}/t_{\rm c} < 1$ and unstable otherwise. Thus for a uniform field strength B_0, any cross-field column of H less than $4 \times 10^{21}{\rm cm}^{-2}(B/10\mu{\rm G})$ will be cross-field stable. This borderline-stable column is consistent with the observed column density seen for many clouds (Larson (1981)) provided the field strength $B \approx 25\mu$G. The cross-field stability criterion $t_{\rm A}/t_{\rm c} < 1$ is equivalent to the requirement that the mass-to-flux ratio in a sphere carved out of this medium satisfy $M/\Phi < 1/(3G^{1/2})$.

For density perturbations with wavevectors parallel to the mean field $\mathbf{B}_0$, the Jeans gravitational stability analysis including just thermal gas pressure is incomplete if, as has

been proposed, Alfvén waves provide the primary cloud support along the mean field. In quasilinear theory (cf. Dewar (1970), McKee & Zweibel (1995)), we can estimate the importance of waves in opposing gravitational collapse along $\hat{\mathbf{B}}_0$ by performing a Jeans-type analysis with $\hat{k} \parallel \hat{\mathbf{B}}_0$ and pressure supplied by Alfvén waves according to $P_{\rm wave} = P_{\rm wave,0}(\rho/\rho_0)^{1/2}$ (assuming $t_{\rm A} \ll t_{\rm c},\ t_{\rm s}$). Here, $P_{\rm wave,0} \equiv |\delta\mathbf{B}|^2/8\pi$ is the pressure in the fluctuating field, and we assume Alfvén wavelengths short compared to the wavelength of the density disturbance. Defining the Jeans number $n_{\rm J} \equiv L/L_{\rm J}$, the criterion for stability on a scale L works out to be

$$n_{\rm J} < \left(1 + \frac{E_{\rm W}}{4\bar{\rho}Lc_{\rm s}^2}\right)^{1/2}, \tag{6}$$

where the Alfvén wave surface energy density is $E_{\rm W} = \int dx \frac{1}{2}(\rho|\delta\mathbf{v}|^2 + |\delta\mathbf{B}|^2/4\pi) = L\langle|\delta\mathbf{B}|^2\rangle/4\pi$.

An extension of the above quasilinear theory to the nonlinear regime ($E_W \gg \bar{\rho}Lc_{\rm s}^2$) would argue that for arbitrary $n_{\rm J}$, clouds could be stabilized against collapse along $\hat{\mathbf{B}}_0$ whenever there is sufficient wave energy (in the absence of wave decay). Properly, we do not expect the analysis above to extend to the nonlinear regime (indeed, while our nonlinear simulations do show correlations of wave pressure and density, they do not obey any simple law like $P_{\rm wave} \propto \rho^{\gamma_p}$). However, *any* argument that balances wave energy in the slab against gravitational potential energy – for example, a virial analysis – will yield the same scaling as equation (6), since binding energy is proportional to $n_{\rm J}^2\bar{\rho}Lc_{\rm s}^2$ (see eq. [26]). The result of Pudritz (1990) is the same as equation (6) up to the factor 1/4. Since our simulations begin from uniform conditions, we find it convenient to use the quasilinear-theory prediction of equation (6) as a reference point. Of course, this "pseudo-Jeans" analysis, or any analysis in terms of an *initial* wave energy, becomes inapplicable if random motions dissipate rapidly compared to the collapse timescale.

2.3. Wave Dissipation Mechanisms

The dominant linear damping mechanism in molecular clouds is ambipolar diffusion (see McKee et al. (1993) and references therein). Ambipolar diffusion prevents propagation of Alfvén waves with frequencies $\omega_A = \mathbf{k} \cdot \mathbf{v}_{\rm A}$ higher than a critical frequency $\omega_c = 2\nu_{ni}$, where the neutral-ion collision frequency is $\nu_{ni} \sim n_i\, 1.5 \times 10^{-9}{\rm cm}^3 s^{-1}$ (Kulsrud & Pearce (1969), Nakano (1984)). Estimates of ν_{ni} indicate that waves can propagate at wavelengths well below 0.01pc (Myers & Khersonsky (1995)). Ambipolar diffusion also damps Alfvén waves with $\omega_A < \omega_c$ at a rate $\dot{E}_{\rm W}/E_{\rm W} = -\omega_A^2/\nu_{ni}$. Writing the ionized fraction as $n_i/n_H = Kn_H^{-1/2}$, the ambipolar-diffusion damping time for wavelengths λ is shorter than

the gravitational collapse time t_c when

$$\lambda < 14 \left(\frac{K}{10^{-5}\mathrm{cm}^{-3/2}}\right)^{-1/2} \left(\frac{\beta}{0.01}\right)^{-1/2} \left(\frac{T}{10\mathrm{K}}\right)^{1/2} \left(\frac{n_{H_2}}{10^2\mathrm{cm}^{-3}}\right)^{-1/2} \mathrm{pc}. \quad (7)$$

For ionization principally by cosmic rays at the fiducial rate $10^{-17}s^{-1}$, $K \sim 10^{-5}$ (McKee et al. (1993)), which for typical parameters can imply significant frictional damping on dynamical timescales for all wavelengths. Including the ionization produced by UV photons increases K and therefore decreases the frictional damping rate. For $\beta < 1$, fast MHD waves frictionally decay at a rate comparable to Alfvén waves. Slow MHD (essentially acoustic) waves suffer little frictional decay, but may be subject to other linear dissipation such as radiative damping.

Nonlinear ($\delta B/B \sim 1$) damping rates due to steepening of compressive (fast magnetosonic) and transverse (Alfvénic) isolated MHD wave trains have been compared by Zweibel & Josafatsson (1983). The former steepen at a rate $\lesssim k\delta v$, while the latter steepen at a rate $\gtrsim k\delta v^2/v_A$; transverse waves damp more slowly because pressure variations are second order in the wave amplitude rather than first order. Isolated wave trains deposit their energy in shocks in approximately a wave-steepening time. (Note that parallel-propagating slow MHD waves with $\delta v/c_s \gg 1$ do not exist; they shock immediately.) Because Alfvén waves have the lowest nonlinear damping rates, it has been suggested that the observed supersonic linewidths owe their existence to these waves (Zweibel & Josafatsson (1983)).

Isolated circularly polarized Alfvén wave trains form a special case because they are exact solutions to the compressible ideal MHD equations and therefore suffer no nonlinear steepening. They are subject to a parametric instability, however, that causes them to excite compressive and magnetic disturbances over a range of ω and k (Goldstein (1978)). The growth rate of the parametric instability is of order the wave frequency when $\beta \lesssim 1$ and the dimensionless amplitude of the wave is of order unity. In the small-amplitude, low-β limit this instability becomes the well-known decay instability (Sagdeev & Galeev (1969)) in which a forward-propagating circularly-polarized Alfvén wave decays into a forward-propagating acoustic wave and a backward-propagating circularly-polarized Alfvén wave. Circularly polarized Alfvén waves cannot be relied upon, therefore, to provide slowly damped motions in molecular clouds.

In truth, many waves are present in a molecular cloud simultaneously, and interactions among waves are as important as the steepening (essentially a self-interaction) of a single wave. Wave interactions transfer energy between scales; when energy is transferred to the smallest scales, dissipation occurs. The energy spectrum that develops depends of course on the allowed wave families in the fluid. The most familiar example of this process is the Kolmogorov cascade in an incompressible, unmagnetized fluid, which leads to an energy

spectrum $dE(k)/dk \propto k^{-5/3}$. For magnetized, incompressible fluids ($c_{\rm s}/v_{\rm A} \gtrsim 1$), a theory of weak turbulence based on coupling of shear Alfvén waves has recently been developed by Sridhar & Goldreich (1995) (SG). The cascade to small scales occurs predominantly perpendicular to the mean magnetic field, but the weak theory becomes invalid at large $k_\perp$ due to increasing nonlinearity. A theory of critically-balanced strong turbulence, again for incompressible media, has been proposed by Goldreich & Sridhar (1995) (GS).

Turbulence in molecular clouds lies in a rather different part of parameter space than that considered by Goldreich & Sridhar, so their theory cannot be directly applied. The SG+GS theory was developed for application to scintillation in the ionized interstellar medium, where $c_s/v_A \gtrsim 1$. In molecular clouds, by contrast, self-gravity and efficient cooling have conspired to produce a highly compressible medium ($c_{\rm s}/v_{\rm A} \ll 1$) in which turbulence is probably strong ($\delta v/v_{\rm A} \sim 1$) at the largest scales. In low-β media, compressive disturbances are easily excited and damp rapidly via shocks. In general, a low-β plasma can be expected to generate both an anisotropic shear-Alfvén cascade, similar to that studied by SG+GS, and compressive disturbances and shocks (cf. Ghosh & Goldstein (1994)). Only with high-resolution two- or three- dimensional numerical studies of compressible MHD turbulence will it be possible to delineate the circumstances when one or the other mechanism provides the primary dissipation for Alfvénic disturbances in conditions appropriate for molecular clouds. In this first study, we have adopted a compressible equation of state but use the the simplest possible geometry (slab symmetry) that allows for transfer of Alfvén -wave energy to compressive motions. Insofar as our model allows for compressibility but not a perpendicular Alfvén -wave cascade, our study is complementary to that of Goldreich & Sridhar.

3. Basic Equations, Numerical Method, and Tests

In this paper we consider the simplest possible system in which nonlinear MHD waves and gravity can interact. We solve the equations of self-gravitating, compressible, ideal MHD:

$$\frac{\partial \mathbf{v}}{\partial t} + (\mathbf{v}\cdot\nabla)\mathbf{v} = -\frac{\nabla P}{\rho} - \frac{\nabla \mathbf{B}^2}{8\pi\rho} + \frac{(\mathbf{B}\cdot\nabla)\mathbf{B}}{4\pi\rho} - \nabla\phi, \tag{8}$$

$$\frac{\partial \rho}{\partial t} = -\nabla\cdot(\rho\mathbf{v}), \tag{9}$$

$$\frac{\partial \mathbf{B}}{\partial t} = \nabla\times(\mathbf{v}\times\mathbf{B}), \tag{10}$$

$$\nabla^2\phi = 4\pi G\rho. \tag{11}$$

The equation of state is isothermal,

$$P = c_s^2 \rho, \tag{12}$$

with $c_s = 1$ throughout.

We assume "slab symmetry", that is, all variables are a function of one independent spatial variable x and time t. Thus derivatives in the transverse (y and z) directions are zero, and the only derivatives that survive in equations (8) to (11) are in the longitudinal (x) direction. Transverse velocities $\mathbf{v}_\perp$ and magnetic fields $\mathbf{B}_\perp$ also survive and vary with x, making our scheme "1 + 2/3 D". Notice that because of the symmetry and the constraint $\nabla \cdot \mathbf{B} = 0$ we have $B_x(x,t) = const$. The boundary conditions are periodic in a slab of thickness $L = 1$, i.e. a fluid element leaving the model at $x = -L/2$ reenters at $x = L/2$. For periodic boundary conditions, $\rho \rightarrow \rho - \bar{\rho}$ on the right-hand-side of equation (11) (see §4.3).

Our numerical method is a one dimensional implementation of the ZEUS code described by Stone & Norman (1992a) and Stone & Norman (1992b). The hydrodynamical portion of the code is a time-explicit, operator-split finite difference algorithm on a staggered mesh. Density and internal energy are zone-centered, while velocity components dwell on zone faces. The magnetic portion of the code uses the Method of Characteristics to evolve the transverse components of the magnetic fields and velocities in a manner that assures the successful propagation of Alfvén waves.

The gravitational acceleration, when used in our model, is calculated by taking the Fourier transform of the density and, for each component of the potential ϕ_k, setting $\phi_k = 4\pi G \rho_k (\Delta x)^2 / (2\cos(k\Delta x) - 2)$, where Δx is the zone spacing. This gravitational kernel ensures that Poisson's equation is satisfied in finite-difference form. The gravitational acceleration is calculated by taking the inverse transform and setting $g_i = -(\phi_{i+1/2} - \phi_{i-1/2})/\Delta x$. We have confirmed that selected spatial modes obey the Jeans dispersion relation as a test of the gravitational portion of the code.

As a further comparison with linear theory, we have verified the scalings $P_{\rm wave} \propto \rho^{3/2}$ and $P_{\rm wave} \propto \rho^{1/2}$ for the Alfvén wave pressure in, respectively, an adiabatically contracting cloud and a wavetrain propagating along a density gradient (McKee & Zweibel (1995)). To verify the first scaling, we imposed a slow contraction of the coordinate system in a simulation containing a low-amplitude Alfvén wave and found good agreement with the adiabatic wave amplitude-density relation. To verify the second scaling, we imposed an external gravitational potential to set up a density gradient and forced a low-amplitude Alfvén wave at the bottom of the potential well. Again, we found that the wave amplitude for the outward-propagating wavetrain agreed well with the linear "polytropic" theory.

While our numerical method thus produces good agreement with linear theory, the experiments we present below involve the evolution of highly nonlinear MHD systems. It is hard to find good code tests for such systems, since there are few exact solutions known. Tests that exercise an MHD code's ability to handle the full family of MHD discontinuities have been described by Ryu & Jones (1995); we have performed these tests and obtained satisfactory results.

Another direct and germane nonlinear test of the code is provided by the parametric instability of circularly polarized Alfvén waves in a compressible fluid described by Goldstein (1978). We have simulated the instability of circularly polarized Alfvén waves and verified that the growing disturbances obey Goldstein's analytic dispersion relation. We have also simulated the steepening of an elliptically polarized Alfvén wave and found good agreement with the calculations of Cohen & Kulsrud (1975).

Finally, we have convergence tested the code for many of the simulations described in this paper. An example is shown in Figure 1, which displays the evolution of "wave" energy (kinetic and magnetic energy) in a suite of simulations that begin with a "random" set of transverse velocities and magnetic fields (see §4.1 for details of the initial conditions). The simulations vary only in their numerical resolution; the initial conditions are identical in the sense that their Fourier transforms are the same. Evidently as resolution increases the energy evolution converges. This is because numerical diffusion decreases as resolution increases, while the real sources of dissipation – isothermal shocks– become increasingly well resolved. Provided we use sufficient resolution (of order 512 zones in this case), the energy evolution will not depend qualitatively or quantitatively on numerical effects.

4. Simulations

We have performed several different types of simulations using the basic model described in the last section: a periodic, one-dimensional system with magnetic fields and an isothermal equation of state. This model may be thought of as mocking up a piece of a molecular cloud that is dominated by a mean field lying in the longitudinal (x) direction, although it also serves as perhaps the simplest possible context in which to study the interaction of Alfvén waves and self-gravity. All the simulations begin with a uniform initial density $\rho = 1$, zero longitudinal velocity ($v_x = 0$), and zero mean transverse field ($\bar{B}_y = \bar{B}_z = 0$; we have verified that small mean transverse fields do not change our results qualitatively). Each simulation can be characterized by the (unchanging) strength of the mean longitudinal magnetic field B_x, expressed in terms of the parameter $\beta \equiv c_{\rm s}^2/v_{\rm A}^2 \equiv c_{\rm s}^2/(B_x^2/4\pi\rho)$ (see eq. [1]; we include only the mean field component B_x in

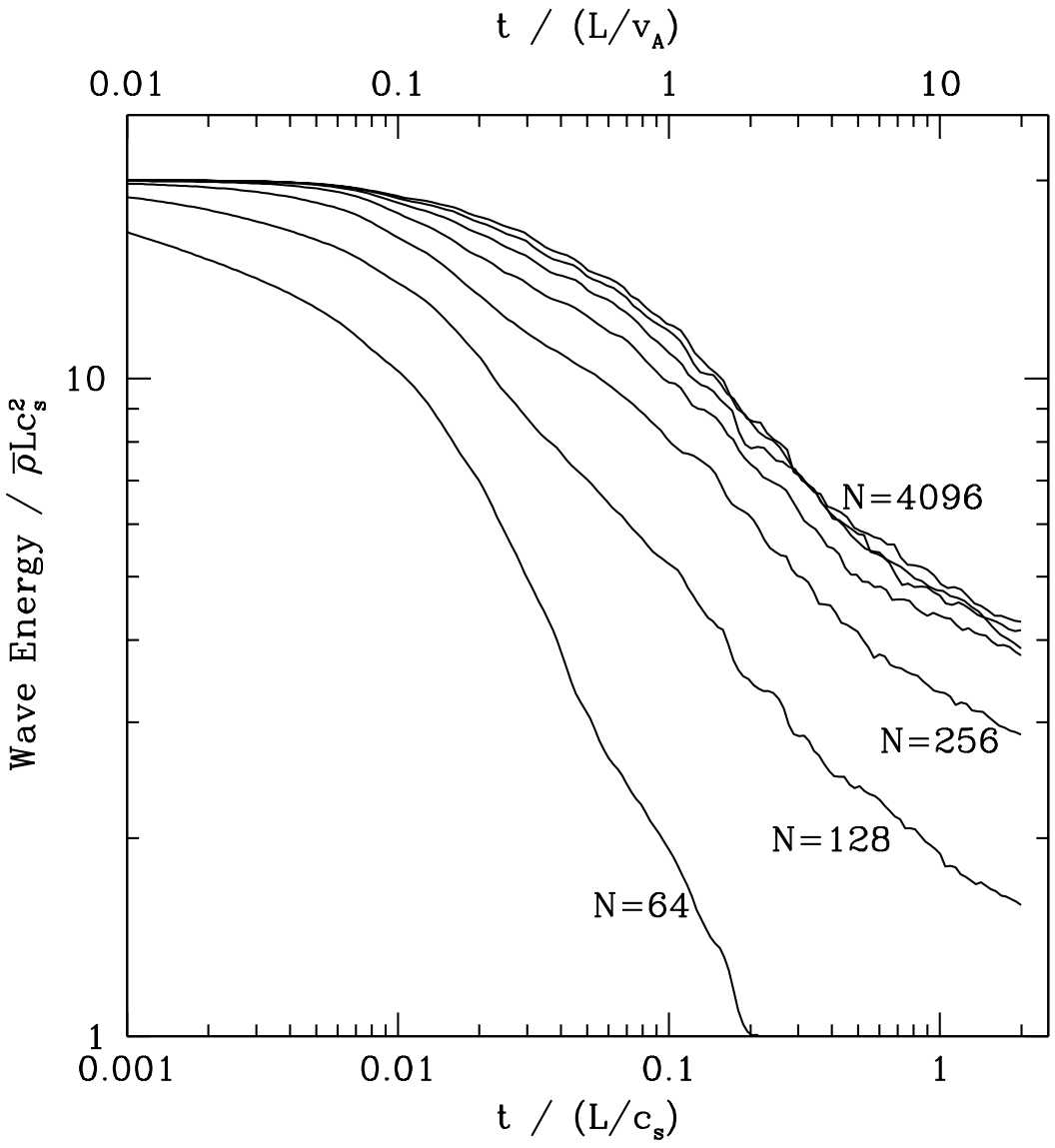

Fig. 1.— A convergence test. The figure shows the evolution of the sum of the magnetic and kinetic energy in simulations that begin with an initially random transverse field and velocity, but with different numerical resolution. This shows that the evolution does not depend on numerical effects for large enough resolution.

$v_{\rm A}$). The numerical resolution for the "standard" runs described below is 2048 zones; all other runs were done with 512 zones. Four different types of simulations are discussed in the subsections below. They are: the free decay of an initial wave spectrum (§4.1); a forced equilibrium in which the model is stirred at the same rate that it dissipates energy (§4.2); the free decay of an initial wave spectrum in the presence of self-gravity (§4.3); and a forced equilibrium in the presence of self-gravity (§4.4).

A useful diagnostic for the simulations described below is what we shall call the *wave energy*. It is defined as the sum of the kinetic energy and the energy of the perturbed magnetic field, $E_{\rm W} = E_{\rm K} + E_{\rm B}$, where

$$E_{\rm K} \equiv \int_{-L/2}^{L/2} dx \frac{1}{2}\rho(|\mathbf{v}_\perp|^2 + v_x^2) \tag{13}$$

and

$$E_{\rm B} \equiv \int_{-L/2}^{L/2} dx \frac{|\mathbf{B}_\perp|^2}{8\pi}. \tag{14}$$

Notice that $E_{\rm K}, E_{\rm B}$, and $E_{\rm W}$ are in units of energy per unit surface area because of the slab geometry. For reference, the rms velocity and magnetic field perturbations satisfy $\langle|\delta\mathbf{v}/c_{\rm s}|^2\rangle^{1/2} = (2E_{\rm K}/\bar{\rho}Lc_{\rm s}^2)^{1/2}$ and $\langle|\delta\mathbf{B}/B_x|^2\rangle^{1/2} = \beta^{1/2}(2E_{\rm B}/\bar{\rho}Lc_{\rm s}^2)^{1/2}$. The definition of β implies that $v/v_{\rm A} = \beta^{1/2}v/c_{\rm s}$ for any v. Time is given in units of the sound-crossing-time $t_{\rm s} \equiv L/c_{\rm s}$, and the Alfvén -wave crossing time $t_{\rm A} = L/v_{\rm A} = t_{\rm s}\beta^{1/2}$. For self-gravitating simulations, the collapse time is $t_{\rm c} = t_{\rm s}/n_{\rm J}$, where $n_J \equiv L/L_J$ (see eqs. [2], [3], and [4]).

4.1. Free Decay

First consider a non-self-gravitating model containing a spectrum of waves in the initial conditions that are allowed to freely decay thereafter. The "standard" run has $\beta = 0.01$ and initial wave energy $E_{\rm W} = 2E_{\rm K} = 2E_{\rm B} = 100\bar{\rho}Lc_s^2$. With this initial energy, the initial field line distortions have a dimensionless amplitude $\langle|\delta\mathbf{B}/B_x|^2\rangle^{1/2} = 1$.

The initial transverse velocities and magnetic fields are a "random" superposition of parallel-propagating Alfvén waves. They are drawn from a Gaussian random field with power spectrum $\langle|\mathbf{v}_{\perp,k}|^2\rangle = \langle|\mathbf{B}_{\perp,k}|^2/4\pi\bar{\rho}\rangle \propto k^{-2}$ for $2\pi/L < |k| < 32(2\pi/L)$. This power spectrum is special in that it approximates the natural power spectrum to which other initial power spectra decay, according to our numerical experiments, and also in that it corresponds to a velocity-dispersion/size relation $\sigma_v(R)^{1/2} \propto R^{1/2}$ in one dimension which is consistent with one of Larson's laws (cf. Larson (1981); §2.1). The power spectrum is steeply declining, so almost all the energy is at the largest scales.

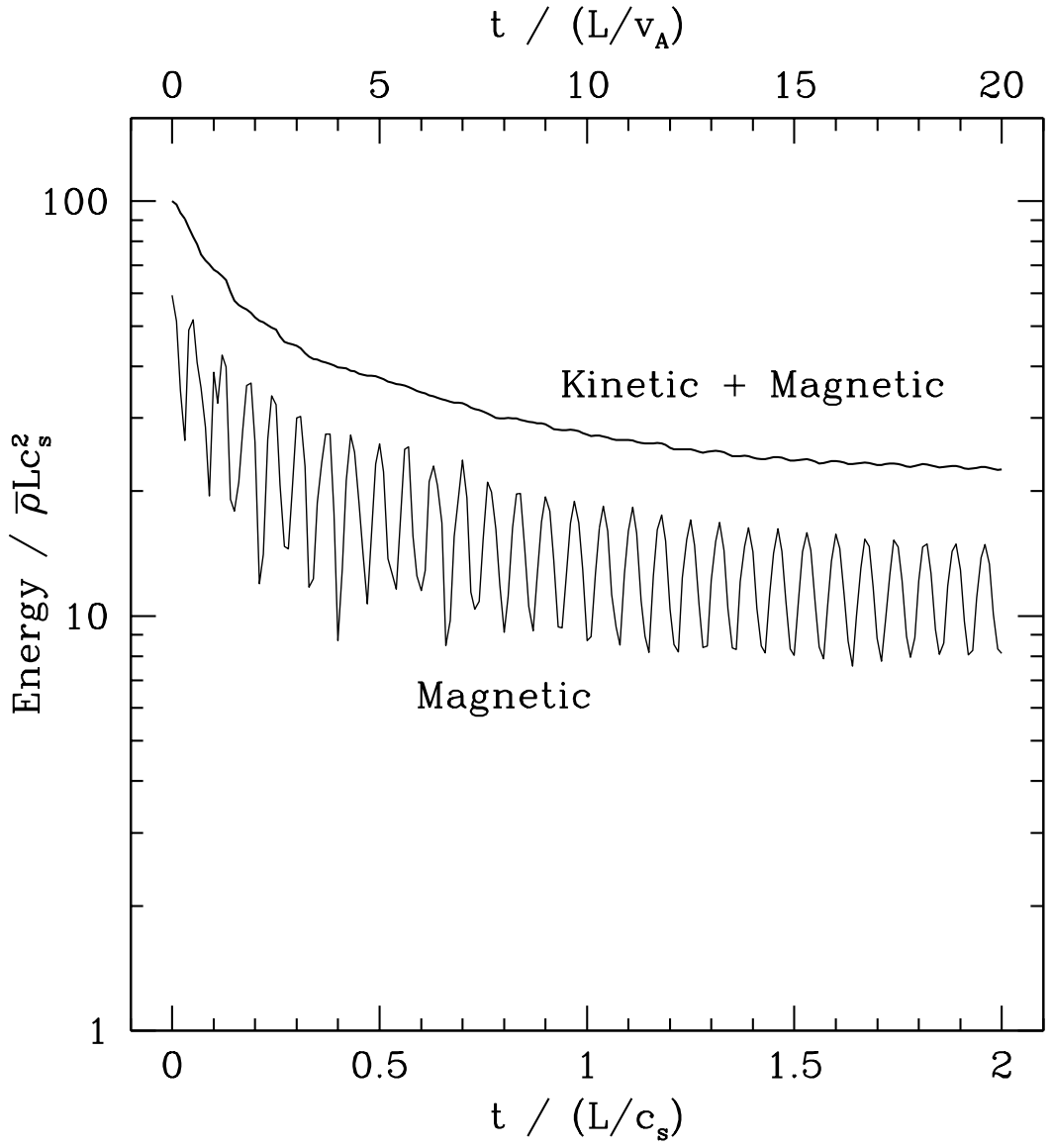

Fig. 2.— Time evolution of the transverse magnetic + kinetic energy and the magnetic energy in the "standard" decay simulation.

The evolution of the total wave energy and the magnetic energy are shown in Figure 2. The initial transverse magnetic fields give rise to a nonuniform magnetic pressure that is large compared to the gas pressure. This in turn produces longitudinal accelerations, in addition to the transverse accelerations caused by magnetic tension. The transverse kinetic and magnetic energies remain nearly in equipartition and oscillate out of phase, yielding a smoothly-evolving total wave energy; the longitudinal kinetic energy is only a few percent of the total. The wave energy declines to half its initial value by $t = 0.2t_{\rm s} = 2.0t_{\rm A}$. The transverse motions and fields lose their energy when the magnetic pressure due to the transverse fields does PdV work on the fluid,

$$\frac{d}{dt}\int_{-L/2}^{L/2} dx \left(\frac{1}{2}\rho|\mathbf{v}_\perp|^2 + \frac{|\mathbf{B}_\perp|^2}{8\pi}\right) = \int_{-L/2}^{L/2} dx\, v_x \frac{\partial}{\partial x}\left(\frac{|\mathbf{B}_\perp|^2}{8\pi}\right), \tag{15}$$

producing longitudinal motions that dissipate in shocks. Toward the end of the simulation almost all the wave energy is concentrated at the largest scales, thus giving the regular oscillations in transverse magnetic energy seen in Figure 2.

Figure 3 shows density, longitudinal velocity v_x, magnetic pressure, and the field line geometry of the simulation at $t = 0.5t_{\rm s} = 5t_{\rm A}$. There are large density contrasts present, with densities ranging over three orders of magnitude. Numerous shocks provide the dissipation. Notice that the magnetic pressure dominates the gas pressure (the gas pressure is numerically equal to the density, since $c_s^2 = 1$). The field line structure in the $x - i$ planes ($i = y, z$) is shown in the lower right panel of the figure, with the i field displacement δ_i defined by

$$\delta_i(x) = \int^x dx\, \frac{B_i}{B_x} - const., \tag{16}$$

where the constant is set so that $\bar{\delta_i} = 0$. Because most of the energy remains in the largest-scale Fourier components of the field, the field displacements are well ordered, with one maximum and one minimum. The field lines are nearly straight, and hence force-free, in between the kinks at density maxima.

The variations in density at $t = 0.5t_{\rm s} = 5t_{\rm A}$ can be further characterized by computing the fractional volume and fractional mass at $\rho > \rho_c$ (Figure 4). The figure shows that 10% of the mass (volume) is at $\rho > 9.1\bar{\rho}$ ($2.7\bar{\rho}$), 50% of the mass (volume) is at $\rho > 3.1\bar{\rho}$ ($0.42\bar{\rho}$), and 90% of the mass (volume) is at $\rho > 0.55\bar{\rho}$ ($0.012\bar{\rho}$). Thus the mass is concentrated in dense regions, while a significant fraction of the simulation volume is nearly empty. These results are typical of all our simulations, although density contrast increases significantly in the self-gravitating simulations discussed below.

At time $t = 0.5t_{\rm s} = 5t_{\rm A}$, the best-fit slope s to the combined power spectrum $|\mathbf{v}_{\perp,k}|^2 + |\mathbf{B}_{\perp,k}|^2/4\pi\bar{\rho} \propto k^{-s}$ yields $s = 2.3$ between $k/(2\pi/L) = 1$ and 100. The slope

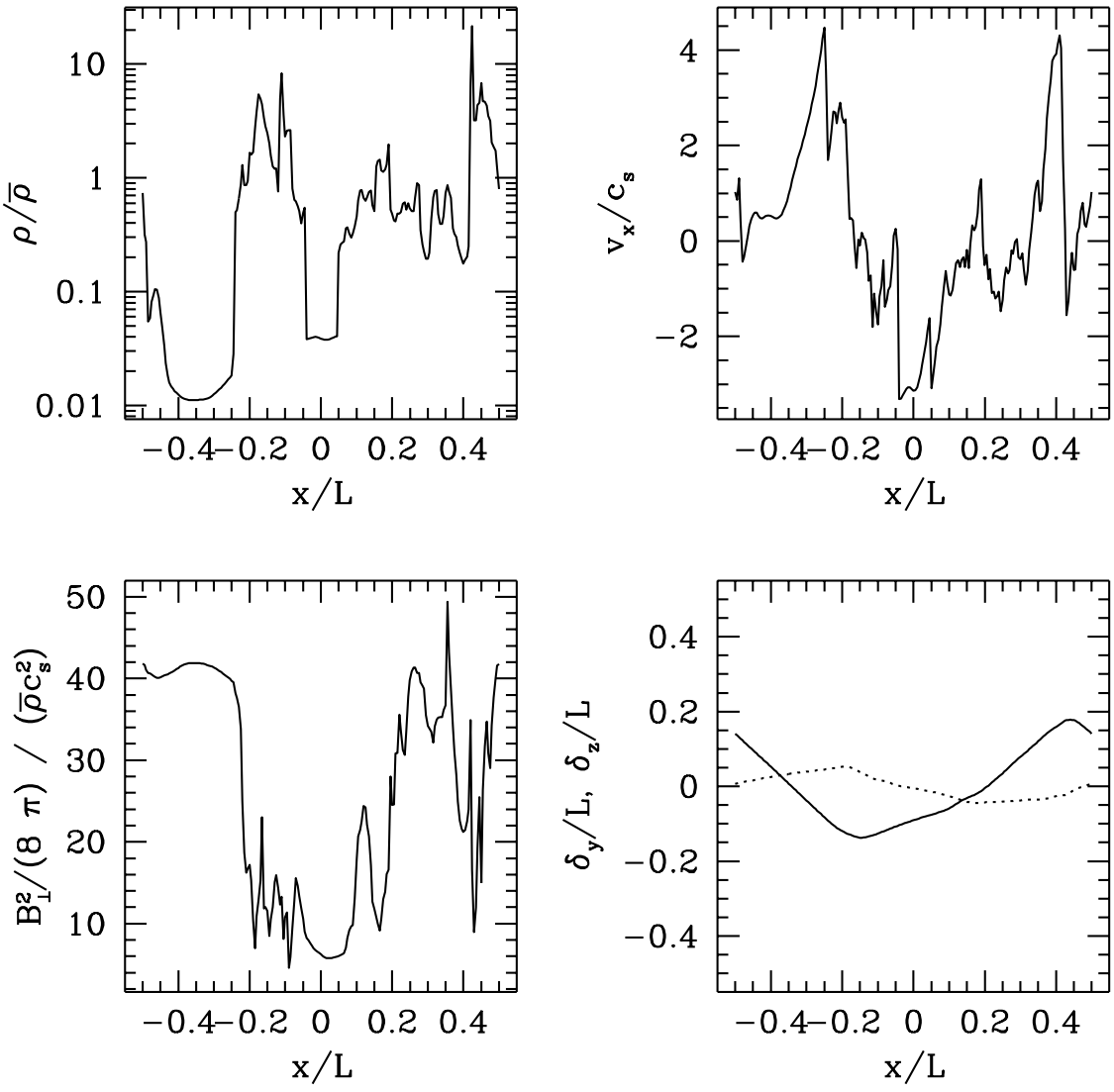

Fig. 3.— Portrait of density ρ, longitudinal velocity v_x, transverse magnetic pressure $B_\perp^2/8\pi$, and transverse field line displacements δ_y, δ_z in the "standard" decay simulation at time $t = 0.5t_{\rm s} = 5t_{\rm A}$.

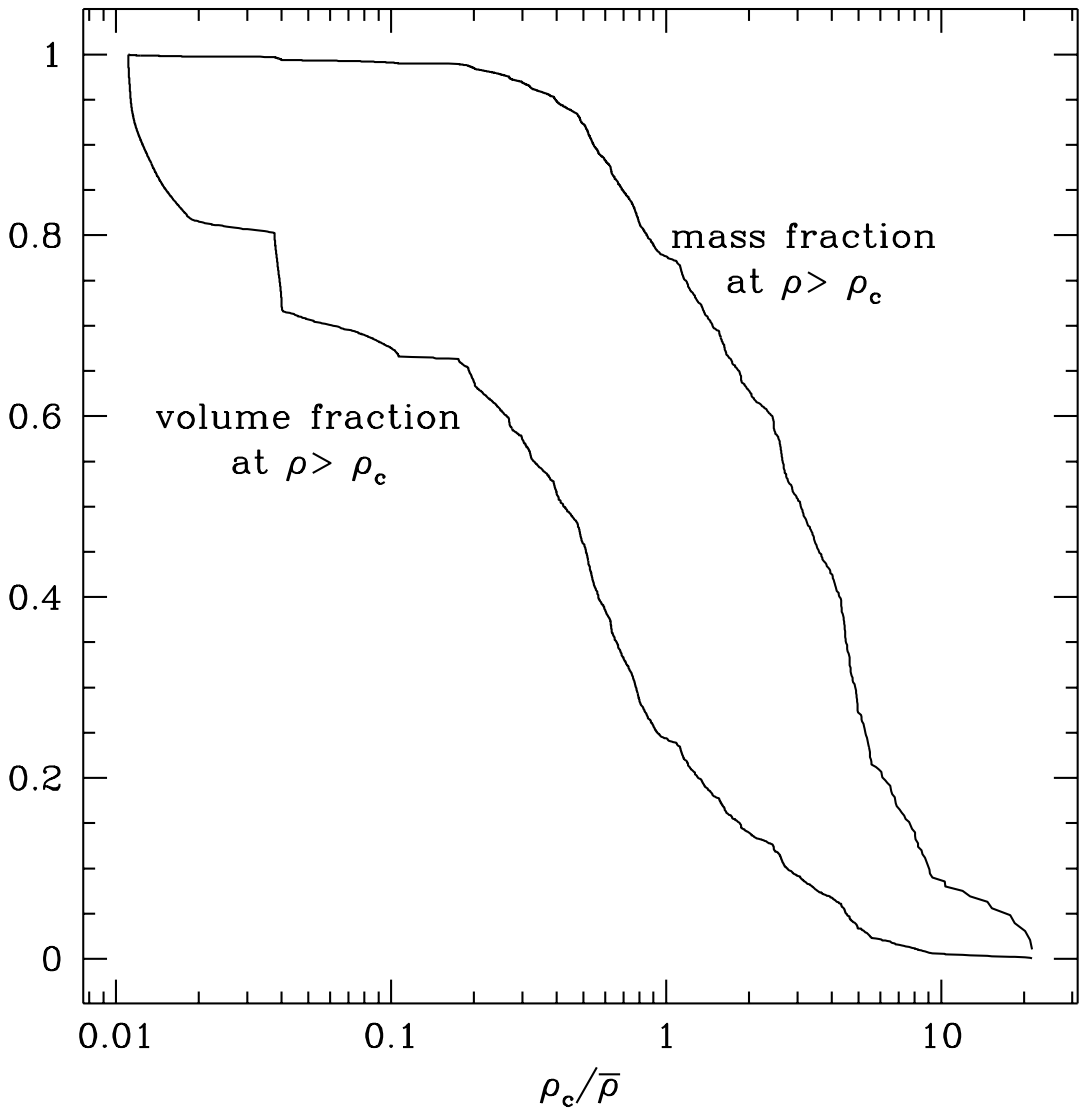

Fig. 4.— Volume and mass fractions above density enhancement level $\rho_c/\bar{\rho}$, for the "standard" decay simulation at time $t = 0.5t_s = 5t_A$.

varies rapidly, however, with $\langle s \rangle = 2.4 \pm 0.16$, where $\langle\rangle$ indicates an average over time. By smoothing the $\mathbf{v}_\perp$ data over Gaussian windows of varying width and averaging over the box, and over time, we can compute a simulated "linewidth-size" relation (see §4.2). Averaged over time, the best fit relation is $\sigma_v(R) \propto R^{0.7}$.

A vital question for the structure of molecular clouds is whether the wave energy concentrates in the regions of highest density. This can be answered by comparing $|\delta\mathbf{B}|^2$ with ρ after smoothing both on a scale λ. In our standard decay simulation, magnetic pressure and density are weakly *anti*correlated in a time-averaged sense, with slope $|\delta\mathbf{B}|^2 \propto \rho^{-0.1}$ for essentially all smoothing scales λ (in §4.3 we show that self-gravity changes this correlation). Thus magnetic pressure plays a role in confining the "clumps". But the clumps are not in equilibrium: they form, disperse, and accelerate, and material migrates from one clump to another. We do find that clump masses grow over time, however, as energy is transferred to larger scales and more coherent motions.

We have surveyed free decay models with the same initial power spectrum over a variety of β and initial E_W. The evolution of the wave energy in a selected sample of these simulations is shown in Figure 5a. The initial dimensionless wave amplitudes range from $\langle|\delta\mathbf{B}/B_x|^2\rangle^{1/2} = 1/4$ to 8. Considering the subset of simulations where the initial rms field perturbations $(\beta E_{\rm W}/\bar{\rho}Lc_{\rm s}^2)^{1/2}$ are 2 or less, for a given initial $E_{\rm W}$ the decay is slower as the field strength increases (β decreases). For this same set of simulations, when we consider decays at a given β, the fractional energy loss at $t_{\rm A}$ increases as initial $E_{\rm W}$ increases.

Some of the simulations with initial wave energy of $400\bar{\rho}Lc_s^2$ stop decaying near the end of their run. This is because they are able to make their way into a special dynamical state. In this special low-decay state, all the matter is concentrated into two narrow sheets that oscillate transversely. This special state is artificial, because its stability depends on the boundary conditions. We have tried duplicating the special state into a region of length $2L$, so that there are four narrow sheets, and introducing some small perturbations. We find that the system becomes unstable and decays to a new special state with only two sheets. The special state may also suffer higher dimensional instabilities which cannot be represented in the present simulations. While our simulations display a common trend toward concentration of energy and structure at the largest available scales, it seems unlikely that suitable conditions for the persistence of this state will be found in nature.

It is not possible to define a "decay rate" from the free decay simulations because the decay rate depends both on the energy and on the internal state of the system. This is made clear in Figure 5b, which shows the instantaneous decay rate $-\dot{E_{\rm W}}/E_{\rm W}$ for the same runs shown in Figure 5a. The heavy black squares indicate where the simulations begin; the decay rates quickly rise, then the energies and the decay rates fall. Except for initial

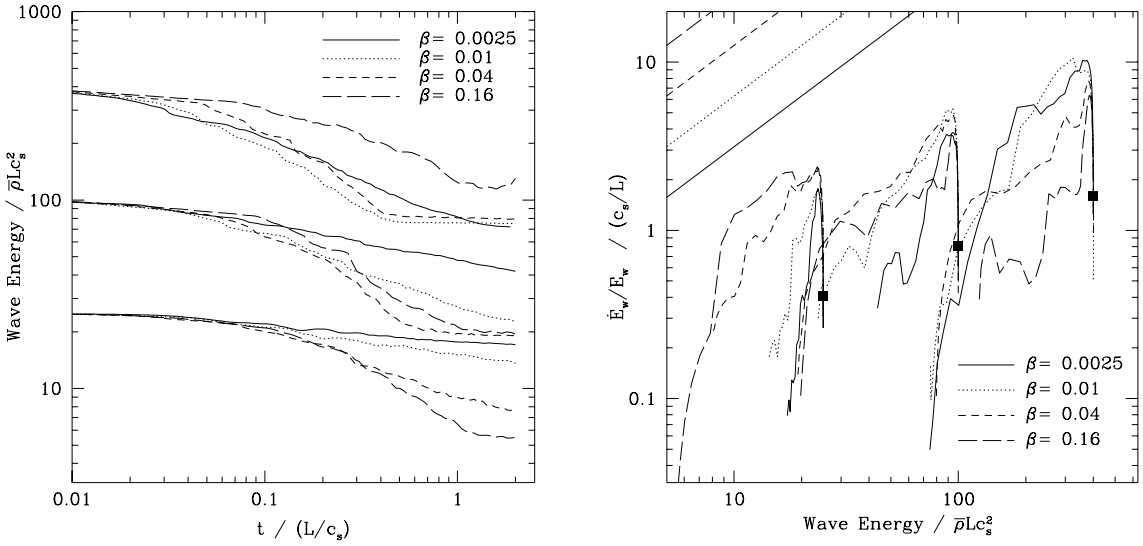

Fig. 5.— (a) Time evolution of the magnetic+kinetic energy in a series of decay simulations with initial wave energy (transverse kinetic + transverse magnetic) of $25, 100$, and 400, and initial $\beta \equiv c_{\rm s}^2/v_{\rm A}^2 = 0.04, 0.01$, and 0.0025. The Alfvén time is $t_{\rm A}/t_{\rm s} = 0.05, 0.1, 0.2, 0.4$ for $\beta = 0.0025, 0.01, 0.04, 0.16$, respectively. (b) The dissipation rate $-\dot{E_{\rm W}}/E_{\rm W}$ as a function of $E_{\rm W}$ in the same simulations as (a). The simulations begin in the neighborhood of the solid black square. The dissipation rate initially increases, then decreases, as the simulations evolve and energy decays. Toward the end of many of these simulations the dissipation rate is sharply reduced because most of the power is in the lowest order ($k = 2\pi/L$) Fourier mode, which decays very slowly. The scale on the ordinate gives the decay rate in units $t_{\rm s}^{-1}$. For $\beta = 0.0025, 0.01, 0.04, 0.16$, a decay rate $t_{\rm A}^{-1} = 20, 10, 5, 2.5 t_{\rm s}^{-1}$, respectively. The straight lines show single wave steepening rates based on Cohen & Kulsrud (1974).

transients in a few of the high-β, high-$E_{\rm W}$ cases, decay rates lie below $t_{\rm A}^{-1}$.

In Figure 5b, the straight lines show the nonlinear decay rate $-\dot{E}_{\rm W}/E_{\rm W} = 2\pi(E_{\rm W}/\bar{\rho}Lc_{\rm s}^2)\beta^{1/2}t_{\rm s}^{-1}$ based on the single-wave steepening calculation of Cohen & Kulsrud (1975), which has sometimes been used to estimate the dissipation rate within molecular clouds. This nonlinear steepening rate overestimates the decay rates we find by an order of magnitude or more, and does not display the same scaling as either the peak decay rates for different runs at a given β, or the evolutionary decay rate for any given run. Indeed, one would not expect the Cohen & Kulsrud estimates to agree with our simulations, since: (a) the simulations contain a spectrum of waves, while the CK estimate is for a monochromatic wave train; (b) the disturbances in our simulations are highly nonlinear at the outset– they do not gradually steepen from a near-mode of the plasma. To the extent that a single decay rate γ can characterize these freely-decaying systems as a function of $E_{\rm W}/\bar{\rho}Lc_{\rm s}^2$ and β, we note that the upper envelope of the decay rate in Figure 5b has better consistency with the scalings and approximate magnitude of the decay rate measured in the steadily forced simulations of the next subsection.

The dissipation rate depends strongly on the initial power spectrum. We have performed a series of simulations with $|\mathbf{v}_{\perp,k}|^2 = |\mathbf{B}_{\perp,k}|^2/(4\pi\bar{\rho}) \propto k^{-2}$ for $k_{\rm min} < k < k_{\rm max}$ and 0 elsewhere, where $k_{\rm min}/(2\pi/L) = 1, 2, 4, 8$, and 16 and $k_{\rm max}/(2\pi/L) = 64$. In all cases $\beta = 0.01$. The time evolution of the wave energy in these simulations is shown in Figure 6; evidently the smaller the scale at which the energy is injected the more rapid the dissipation. The peak decay rates are $\simeq 0.2\omega_A$. Our examination of the evolution of the density and field structure, and the power spectra of the transverse velocities and field (not shown), shows that while energy is lost overall, some fraction of the energy is transferred to modes with k smaller than the initial $k_{\rm min}$. The final power spectra have $|\mathbf{v}_{\perp,k}|^2, |\mathbf{B}_{\perp,k}|^2 \propto k^{-2.5\pm0.2}$ independent of where the cutoff $k_{\rm min}/(2\pi/L)$ was imposed in the input spectrum. We have also initiated decay simulations with alternative spectral slopes, and found that they too evolve toward spectra with slopes in the range -2 to -2.5.

4.2. Forced Equilibrium Runs

The MHD waves in molecular clouds may be trapped and preserved from the time of cloud formation, and the free decay simulations are designed to model that possibility. An alternative, however, is that they are continuously driven by processes inside the cloud, such as winds from young stars (Norman & Silk (1980)). In this section we consider stochastic driving of transverse motions as a model for this process.

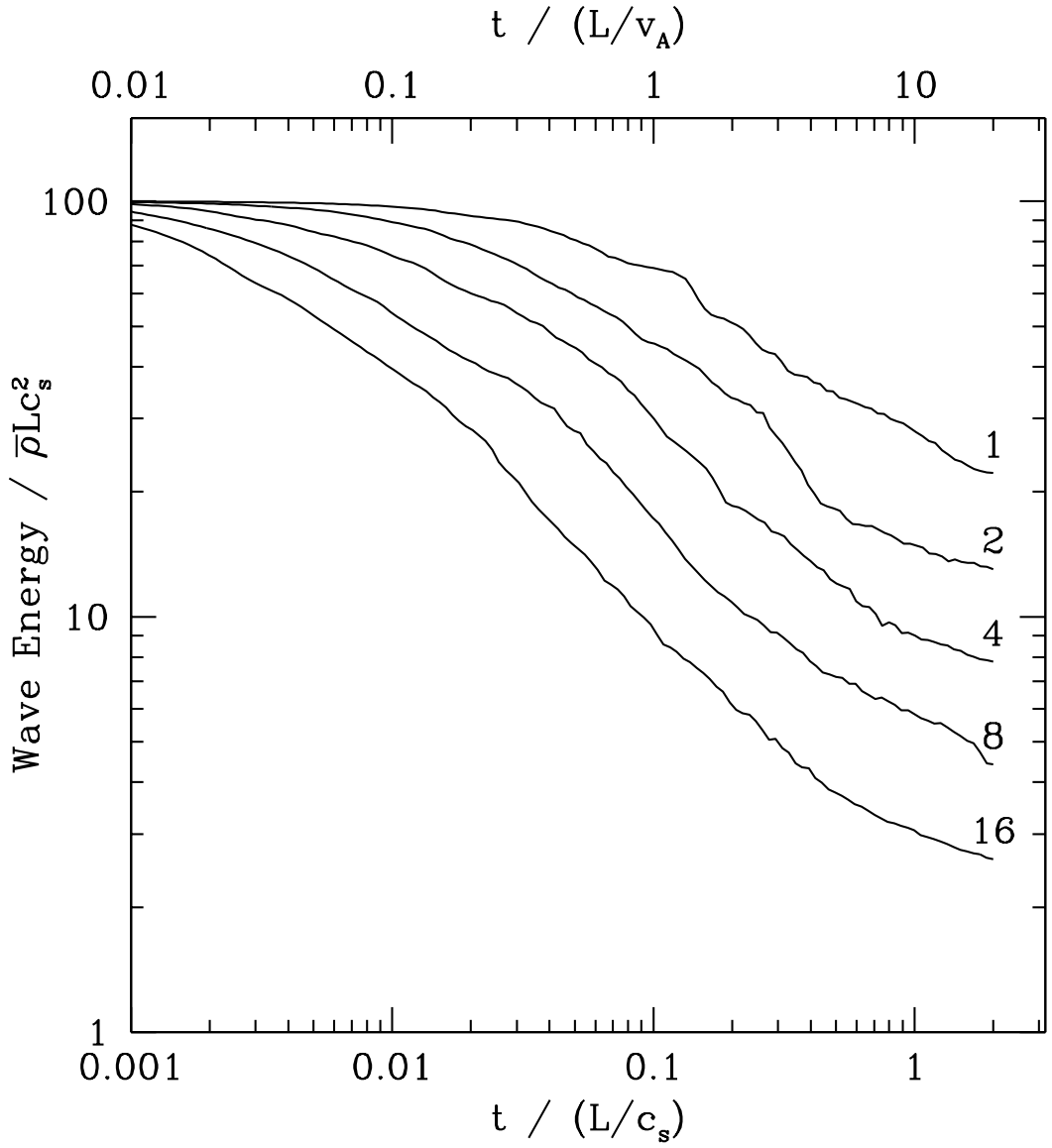

Fig. 6.— Time evolution of the wave energy (kinetic + transverse magnetic) in decay simulations where the initial energy power spectra extend between $k_{\rm min}/(2\pi/L) = 1, 2, 4, 8, 16$ (see labels) and $k_{\rm max}/(2\pi/L) = 64$. The figure demonstrates that decay proceeds more quickly when wave energy is stored in smaller-scale, higher-frequency oscillations.

The forcing is accomplished by introducing a pattern of transverse velocity perturbations $\delta\mathbf{v}_\perp$ at regular time intervals δt. The velocity perturbations have the following properties: (1) $|\delta\mathbf{v}_{\perp,k}|^2 \propto k^4 \exp(-4k/k_{\rm pk})$, so that the power spectrum is peaked at $k = k_{\rm pk}$; (2) the phases of the Fourier components of the perturbation are random; (3) the power spectrum is normalized and the mean component of the transverse velocities set so that

$$\delta E = \int dx \frac{1}{2}\rho \left(|\mathbf{v} + \delta\mathbf{v}|^2 - |\mathbf{v}|^2 \right) = const. \tag{17}$$

and

$$\int dx \rho \delta\mathbf{v} = 0. \tag{18}$$

The forcing interval δt is typically set to be one one-hundredth of a sound crossing time, while $k_{\rm pk}$ is $8(2\pi/L)$ unless stated otherwise.

The evolution of the standard forced run in shown in Figure 7, for which $\beta = 0.01$ and the forcing power $\delta E/\delta t = 100\bar{\rho}c_s^3$. The model equilibrates within a fraction of a sound crossing time. The steady state contains large density fluctuations, as in the free-decay runs. As in the free decay runs, the velocity and magnetic field power spectra evolve toward approximately $\propto k^{-2}$ (even though the model is forced at a scale well below the box size). The best fit slope for the combined power spectrum is $s = 2.2 \pm 0.12$, averaged between times $t/t_{\rm s} = 1$ and 5. After saturation, the density power spectrum is flat below $k = 8(2\pi/L)$.

We now turn to the "linewidth-size" relation in our simulations. In molecular clouds, the linewidth-size relation, one of "Larson's laws" (Larson (1981)), is a correlation with the approximate form $\sigma_v(R) \propto R^{1/2}$ between the linear size R of a region and its internal velocity dispersion $\sigma_v(R)$. Any linewidth-size relation is directly related to the power spectrum of the velocity: for $|\mathbf{v}_k|^2 \propto k^{-n-m}$ in m dimensions, we have $\sigma_v(R) \propto R^{n/2}$ (assuming the emissivity of the gas is uniform). Larson's law is then a natural consequence of an $n = 1$ power spectrum. Power spectra with $n = 1$ occur in systems with an ensemble of velocity discontinuities, known as Burger's turbulence, and are observed in the solar wind (Burlaga & Mish (1987)) and in simulations of supersonic hydrodynamic turbulence (Passot, Pouquet, & Woodward (1988),Porter, Pouquet, & Woodward (1992)). The power spectra in our simulations evolve to approximately $|v_{\perp,k}|^2$, $|B_{\perp,k}|^2 \propto k^{-2}$ (independent of the forcing scale). By smoothing with a Gaussian window, we have directly verified the correspondence between the power spectrum and linewidth-size relation. For the standard run we find a linewidth-size relation of the form $\sigma_v(R) \propto R^{0.57\pm0.03}$ between scales $L/512$ and $L/2$.

We have performed a survey of forced runs to measure the saturation energy as a function of β and the forcing power. The results are shown in Figure 8; a fit to the results

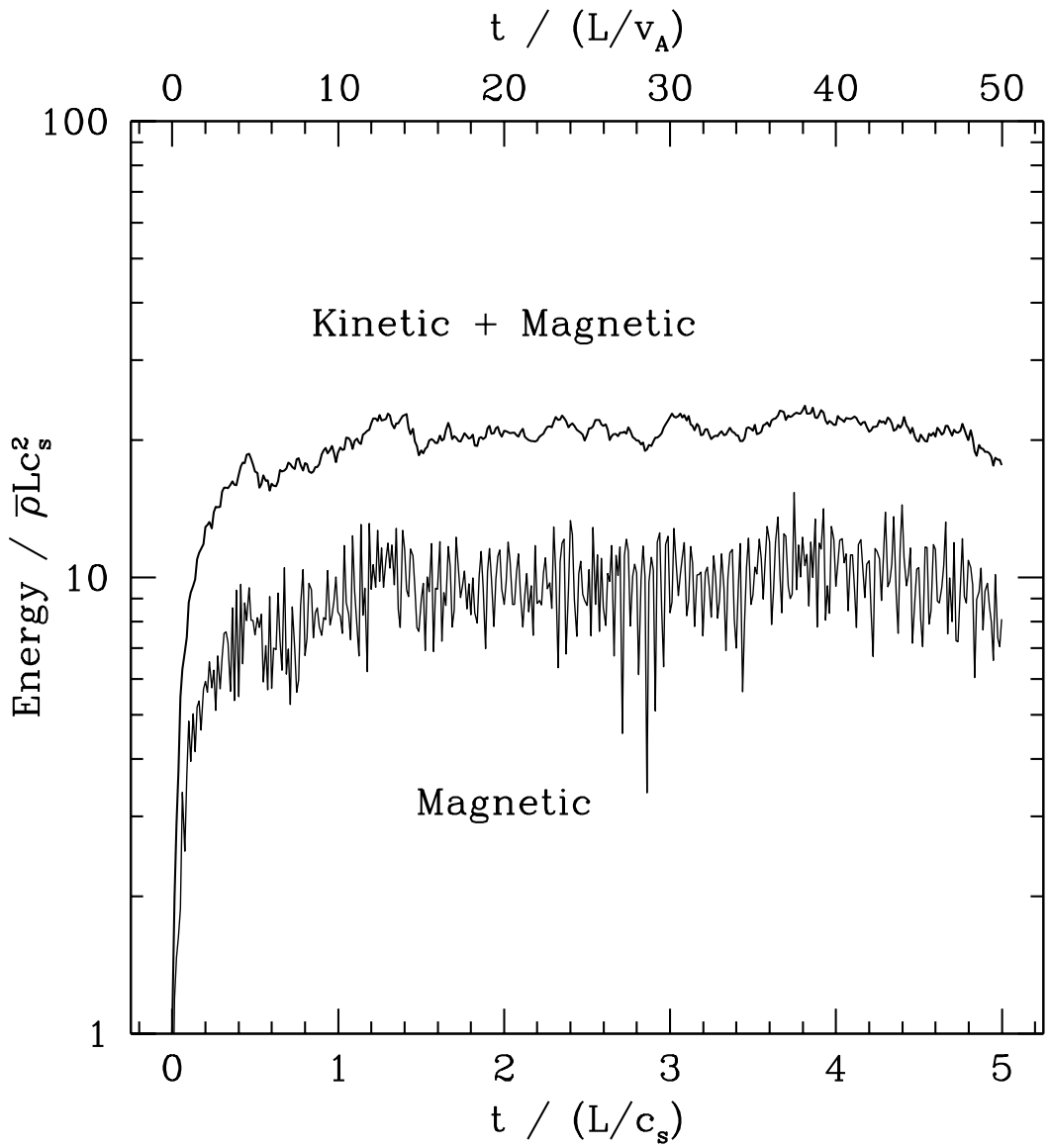

Fig. 7.— Time evolution of the magnetic+kinetic energy and the magnetic energy in the "standard" forced run. The forcing is accomplished by adding random transverse velocities at fixed time intervals.

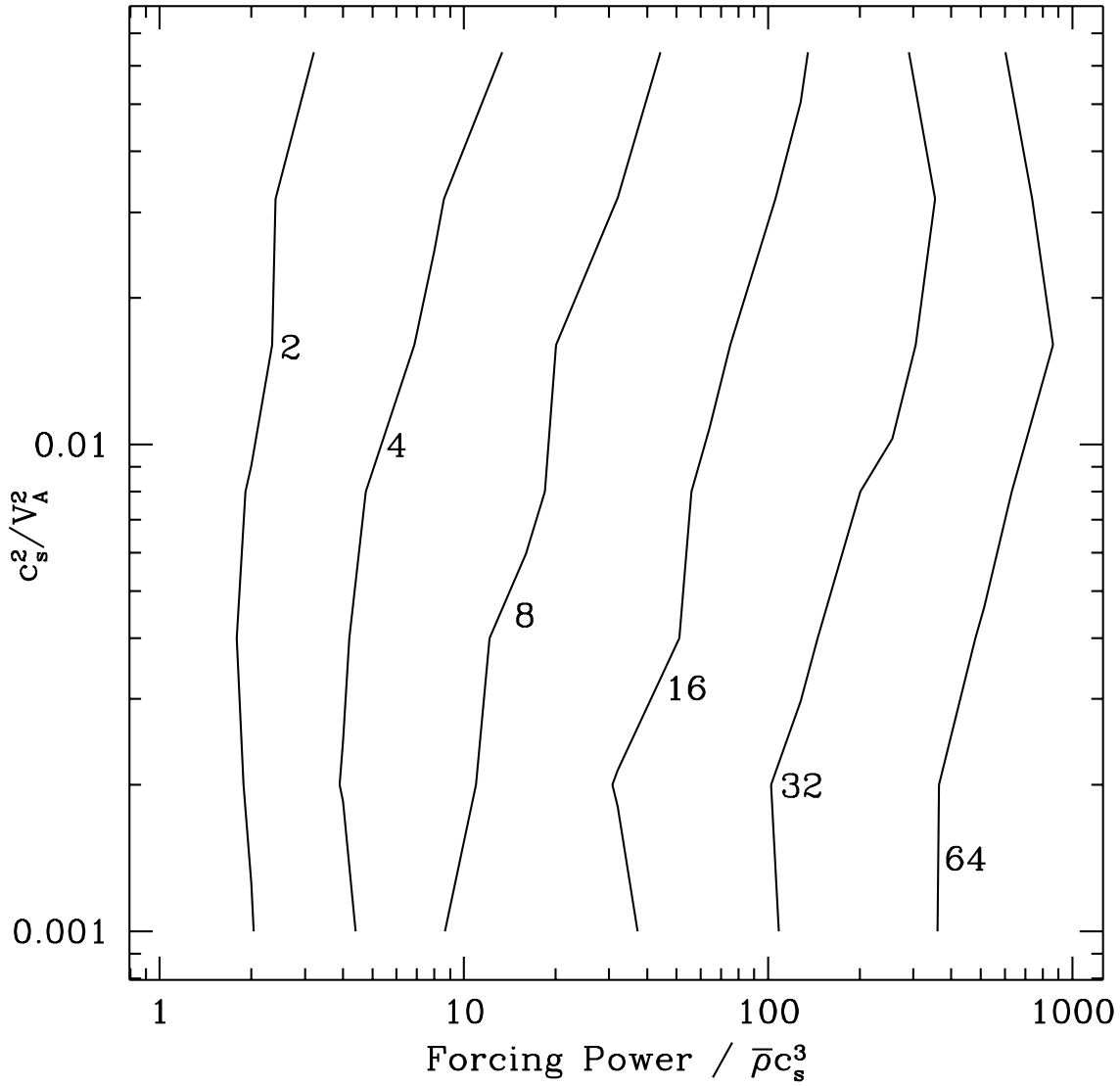

Fig. 8.— A contour plot of the saturation kinetic energy E_K (defined as the average kinetic energy during the final two sound crossing times of the simulation) as a function of the forcing power and $\beta \equiv c_{\rm s}^2/v_{\rm A}^2$. The contours are located at $E_K/(\bar{\rho}Lc_{\rm s}^2) = 2, 4, 8, 16, 32, 64$.

that is better than a factor of 2 everywhere in the region surveyed is

$$E_W = 0.48 \left(\frac{\dot{E}}{\bar{\rho} c_s^3} \right)^{0.67} \beta^{-0.16} \bar{\rho} L c_s^2. \tag{19}$$

We can use the results of Figure 8 to decide what input power is required to sustain a given level of turbulence. Solving for the required power based on the fit above gives

$$\dot{E} = 3.0 \left(\frac{E_{\rm W}}{\bar{\rho} L c_s^2} \right)^{1.5} \beta^{0.24} \bar{\rho} c_s^3. \tag{20}$$

Since the model is in equilibrium the input power matches the dissipation rate.

Notice that, apart from the factor of $\beta^{0.24} \simeq (c_s/v_A)^{1/2}$, the energy dissipation rate per unit volume is $\propto \rho \sigma_v^3 / L$, identical to what one would expect for homogeneous, incompressible turbulence. This is, in part, just dimensional analysis: a dissipation rate per unit volume must have units of a density times a speed cubed over a length. But it is not obvious which speed to use in completing this estimate, since there are three velocity scales in the problem: the sound speed, the Alfvén speed, and the velocity dispersion. The simulations show that the correct speed is a power-law-mean of these three that is dominated by the velocity dispersion.

An example of an alternative scaling for the Alfvén -wave dissipation rate is the estimate of Cohen & Kulsrud (1975) for the steepening of a single wave. The implied energy dissipation rate per unit area is $\dot{E}_{\rm W} \sim 2\pi \left(E_{\rm W} / \bar{\rho} L c_s^2 \right)^2 \beta^{1/2} \bar{\rho} c_s^3$. The corresponding volumetric energy dissipation rate scales as $(\sigma_v / v_{\rm A}) \times (\bar{\rho} \sigma_v^3 / L)$, different from the results of our simulations. Thus the scaling of equation (20) is not a trivial prediction of quasilinear theory, even for compressible magnetized plasmas.

The dissipation rate in the forced runs depends on the wavenumber at which the energy is injected ($k_{\rm pk}$). In the above runs the energy is injected near $k_{\rm pk} = 8(2\pi/L)$. A survey of the dissipation rate as a function of $k_{\rm pk}$ reveals that the saturation energy obeys

$$E_W \propto k_{\rm pk}^{-0.30}. \tag{21}$$

Together with equation(19), this implies that

$$\dot{E} \propto k_{\rm pk}^{0.46}, \tag{22}$$

so that the dissipation rate increases as the forcing scale decreases.

We can define a wave dissipation time $t_{\rm diss}$ in equilibrium by taking the ratio of $E_{\rm W}$ to $\dot{E}$ as given in equation (20). Including the forcing-wavelength dependence of equation (22),

we find

$$t_{\rm diss} \equiv \frac{E_{\rm W}}{\dot{E_{\rm W}}} = 0.87 \left(\frac{\lambda_{\rm pk}}{L}\right)^{0.46} \left(\frac{E_{\rm W}}{\bar{\rho} L c_s^2}\right)^{-1/2} \beta^{-0.24} \frac{L}{c_{\rm s}}. \tag{23}$$

We can compare the dissipation time for forced disturbances to the Alfvén time $t_{\rm A}$ or, for self-gravitating clouds, to the characteristic collapse time $t_{\rm c}$ (eqs. 3, 4). Using $E_{\rm W}/(\bar{\rho} L c_{\rm s}^2) \approx 3\sigma_v^2/c_{\rm s}^2$, the former ratio is $t_{\rm diss}/t_{\rm A} \approx 0.5(\lambda_{\rm pk}/L)^{1/2}(v_{\rm A}/\sigma_v)(v_{\rm A}/c_{\rm s})^{1/2}$; this ratio is generally large unless the forcing scale is very small. Similarly, $t_{\rm diss}/t_{\rm c} \approx 0.5(\lambda_{\rm pk}/L)^{1/2}(v_{\rm A}/c_{\rm s})^{1/2}(n_{\rm J} c_{\rm s}/\sigma_v)$; note that a ratio smaller than unity does not necessitate collapse (see §4.3).

4.3. Self-Gravitating Decay Runs

A crucial question for the evolution of molecular clouds is whether the nonlinear MHD waves interact with the self-gravitating compressive modes (here generically referred to as "Jeans modes") so as to prevent or delay collapse. We can examine this issue by turning on self-gravity in our simulations.

Let us start with a few preliminary words about self-gravity in a periodic slab geometry. First, in one-dimensional, slab geometry an isothermal fluid always has a stable equilibrium, whereas in three dimensions a self-gravitating, isothermal fluid sphere is not generally stable (see Spitzer (1968)). In non-periodic slab geometry, the equilibrium self-gravitating, isothermal density distribution is

$$\rho = \rho_o {\rm sech}^2(z/z_o), \tag{24}$$

where $z_o = c_s/\sqrt{2\pi G \rho_o}$ (Spitzer (1942)). In one dimension, the self-gravitating slab is the nonlinear outcome of the Jeans instability. Second, periodicity implies an important change in the physics of self-gravity: the adoption of the Jeans "swindle." When we solve Poisson's equation we make no allowance for the self-gravity of the background of material at the mean density. Thus we are really solving the equation

$$\nabla^2 \phi = 4\pi G(\rho - \bar{\rho}) \tag{25}$$

rather than Poisson's equation.

Consider a periodic slab geometry with initially uniform density. The self-gravity is such that there are $n_{\rm J}$ Jeans lengths inside length L. If we assign a binding energy $E_G = 0$ to the state with uniform density, it is possible to estimate the binding energy of the self-gravitating slab under the assumption that the density distribution is very nearly the

same as for a non-periodic self-gravitating slab, equation(24), and that there is only one slab present inside L. The result is

$$E_{G,max} \simeq \left(1 - \frac{1}{6n_J^2} - \frac{n_J^2\pi^2}{6}\right)\bar{\rho}Lc_s^2. \tag{26}$$

This is the equilibrium with the *maximum* possible binding energy for an isothermal fluid in one dimension.

The energy evolution of the standard self-gravitating/decay run, with $\beta = 0.01$, initial wave energy $E_{\rm W} = 100\bar{\rho}Lc_s^2$, and Jeans number $n_{\rm J} = 4$ (so that $E_{G,max} \simeq -25\bar{\rho}Lc_{\rm s}^2$), is shown in Figure 9. [3] The background of transverse waves induces large density fluctuations within an Alfvén crossing time, as in the non-self-gravitating case. These density fluctuations now have a gravitational binding energy, however. The density peaks grow and coalesce until at the end of the run (at $t = t_{\rm s} = 10t_{\rm A} = 4t_{\rm c}$) there are only two peaks. As in the non-self-gravitating case, the field lines kink inside the density peaks and are nearly straight (i.e. force-free) in between. Since $E_G/E_{G,max} \simeq 0.4$ at the end of the simulation, the background of MHD waves evidently can delay collapse.

A more detailed look at the evolution of the density structure in the standard simulation is provided in the right panel of Figure 10, which shows $(\rho/\bar{\rho})^{1/4}$ at intervals of $t_{\rm A} = 0.1t_{\rm s} = 0.4t_{\rm c}$. The density has been raised to the 1/4 power to reduce the contrast. The large density contrast induced by the the initial wave spectrum is evident at the first snapshot; the density maxima coalesce and grow over the course of the simulation. The left panel of Figure 10 shows a nonmagnetic simulation that begins with low amplitude white noise in ρ and v_x. The nonmagnetic simulation provides a control for the magnetic simulation and shows that the presence of transverse MHD waves broaden the existing density maxima and delay or prevent their coalescence over several collapse times.

How are the density and magnetic pressure correlated? As in §4.1, we have smoothed the density and magnetic pressure on a scale λ, taken the logarithm of each, and measured the slope and strength of the correlation over a range of λ. When smoothed on the smallest scales, the density and magnetic pressure are weakly correlated (averaging over time), with $\delta B^2 \propto \rho^{0.1}$. As λ is increased, however, the strength and slope of the correlation increase. When $\lambda = L/5$ the slope and strength of the correlation have approximately doubled. Thus on large scales the Jeans modes and Alfvén waves do tend to interact in such a way as to resist collapse. Because the correlation is weak and variable, however, it is inappropriate to interpret it as an effective polytropic equation of state for the wave pressure.

---

[3] Since $c_s, \bar{\rho}$, and L are fixed, the number of Jeans length is set by manipulating G so that, numerically, $G = \pi n_J^2$.

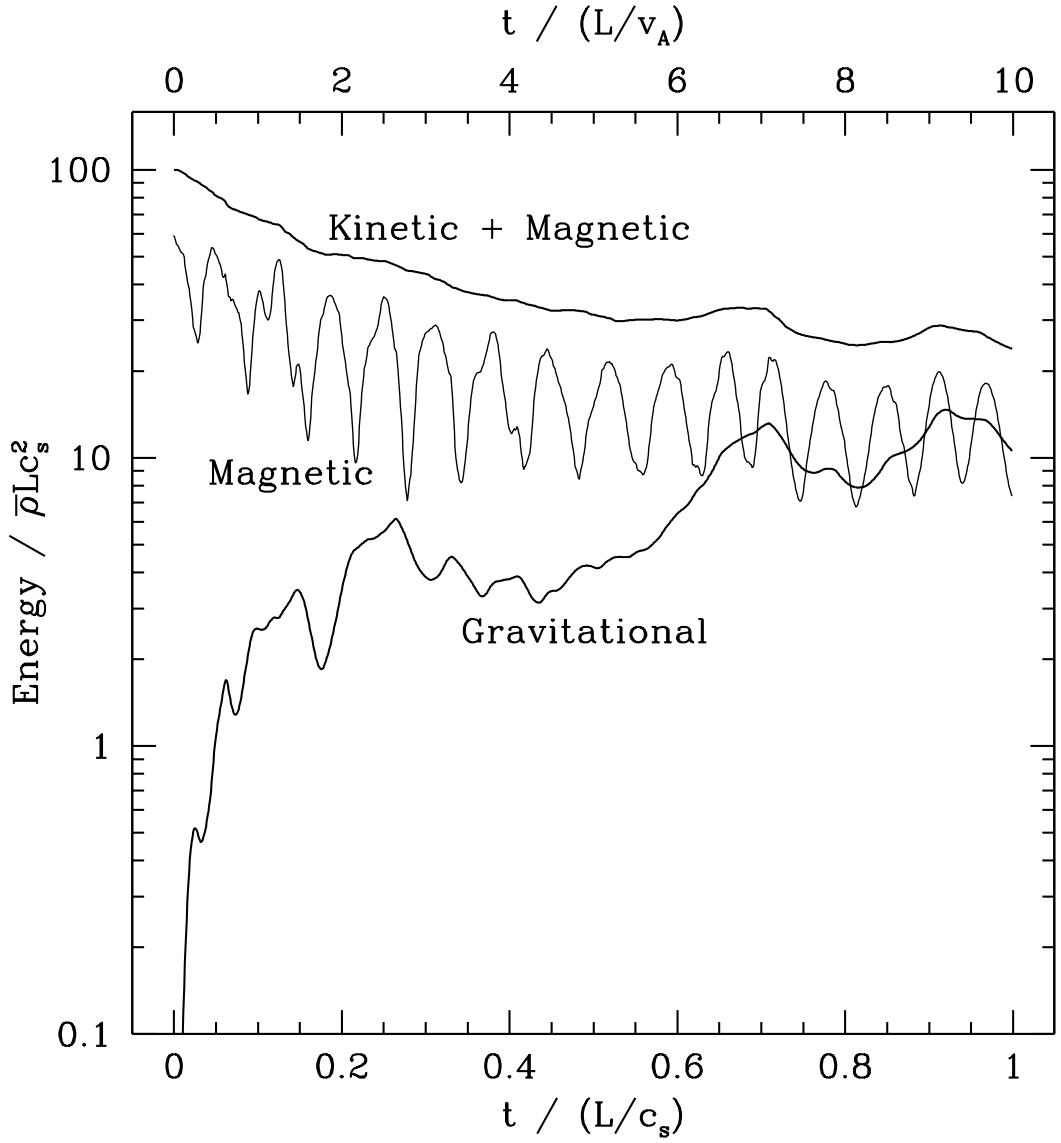

Fig. 9.— Time evolution of the magnetic+kinetic, magnetic, and gravitational potential energy in the "standard" run with decay and gravity. There are four Jeans lengths inside the simulation. Thus $t_{\rm c} = 0.25t_{\rm s} = 2.5t_{\rm A}$.

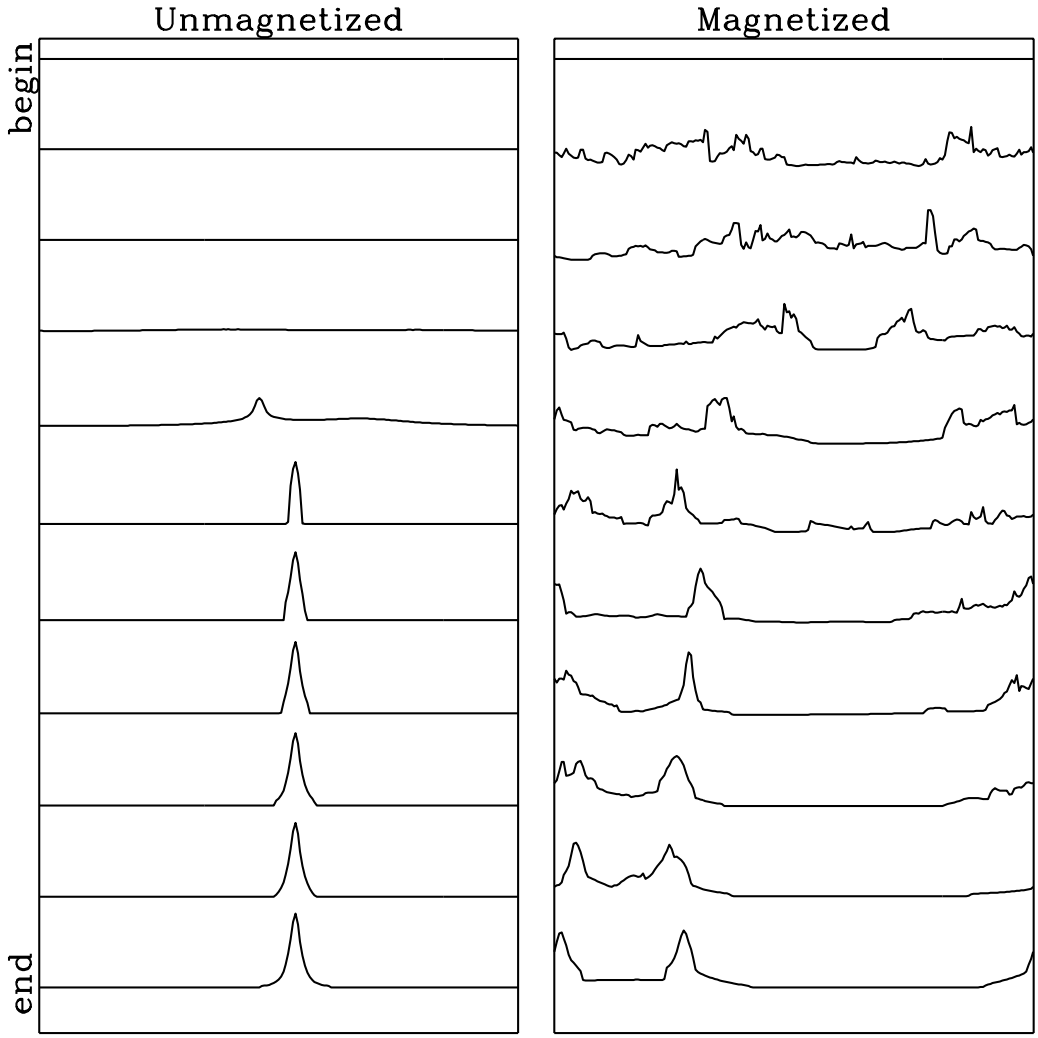

Fig. 10.— Time evolution of the density structure in the "standard" self-gravitating run with decaying wave energy (right panel), and in an unmagnetized control run (left panel). To reduce the contrast, we display $(\rho/\bar{\rho})^{1/4}$ for both cases. Time intervals between the snapshot portraits are $\Delta t = t_{\rm A} = 0.1 t_{\rm s} = 0.4 t_{\rm c}$. The two dense structures which gradually coalesce in the magnetic simulation oscillate in the transverse direction.

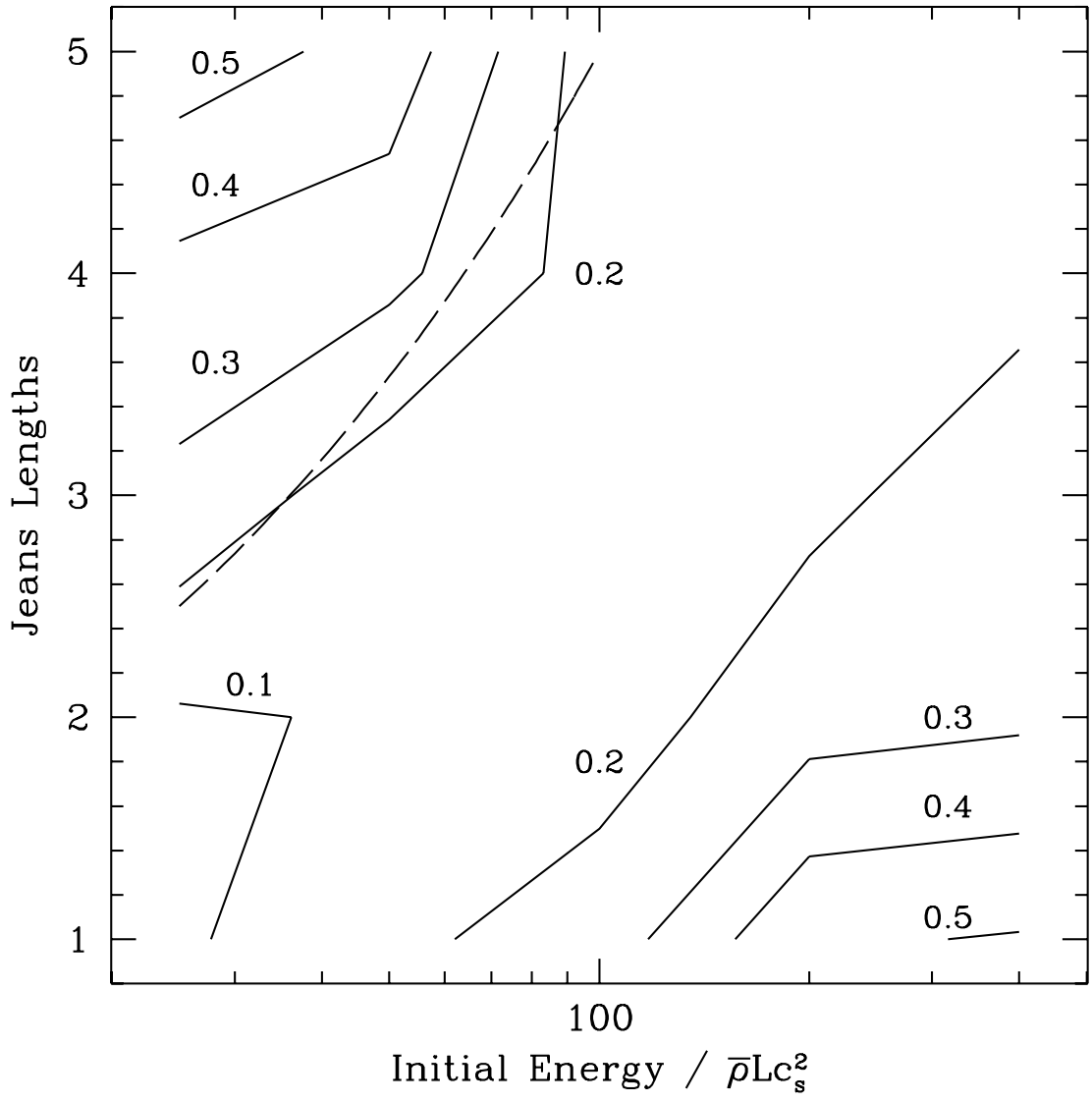

Fig. 11.— A contour plot of the gravitational potential energy $E_{\rm G}$ relative to the maximum gravitational potential energy for a fully-collapsed sheet $E_{\rm G,\,max}$ (eq. 26), averaged between 0.9 and 1.5 $t_{\rm c}$ (the collapse time $t_{\rm c} = t_{\rm s}/n_{\rm J} = 10t_{\rm A}/n_{\rm J}$ for $\beta = 0.01$, where $n_{\rm J} = L/L_{\rm J}$ is the number of Jeans lengths in the simulation) The ratio $E_{\rm G}/E_{\rm G,\,max}$ is measured as a function of the initial magnetic+kinetic energy and $n_{\rm J}$. A large value of $E_{\rm G}/E_{\rm G,\,max}$ corresponds to strong density concentration. The dashed curve shows the locus $n_{\rm J} = (E_{\rm W,\,init}/\bar{\rho}Lc_{\rm s}^2)^{1/2}/2$ (eq. [27]) predicted by the pseudo-Jeans analysis (§2.2) as the lower boundary of the collapsed region. See text for a discussion of the low-$n_{\rm J}$, high-$E_{\rm W}$ part of the diagram.

When can unforced MHD waves prevent gravitational collapse? To investigate this question, we have performed simulations with different initial energies and number of Jeans lengths. We measure the degree of collapse by comparing the time-averaged (from $0.9t_c$ to 1.5 t_c) gravitational binding energy to the gravitational binding energy for a fully collapsed sheet, given by equation (26). Figure 11 shows contours of this ratio ($E_G/E_{G,max}$) as a function of the initial wave energy and the number of Jeans lengths in the simulation.

The maximum in $E_G/E_{G,max}$ in the upper left corner of Figure 11 is where collapse has occurred. This is qualitatively consistent with the pseudo-Jeans analysis of §2.1, which suggests that collapse should occur when the gravitational energy overwhelms the wave energy. Perhaps coincidentally, the pseudo-Jeans analysis is nearly quantitatively correct as well. The dashed line in the Figure shows the locus

$$n_{\rm J} = \frac{1}{2}\sqrt{\frac{E_{\rm W,\,init}}{\bar{\rho}Lc_{\rm s}^2}}, \tag{27}$$

predicted by equation (6), when $E_{\rm W} \gg \bar{\rho}Lc_{\rm s}^2$, as the lower limit in Jeans number for collapse to occur. This locus is indeed close to the boundary of the "collapsed" region. Other simulations show that the structure of this diagram is only weakly dependent on β over the range we have surveyed.

There is also a maximum in $E_G/E_{G,max}$ in the lower right corner of Figure 11. In this region of parameter space the large initial wave motions drive large density fluctuations. These density fluctuations have an associated binding energy, which is large compared to the maximum possible binding energy $E_{G,max}$ because $E_{G,max}$ is small when n_J is small. Thus, while the binding energy is near maximal, the system is not bound because the wave energy is comparatively large.

The scaling with energy of the stability criterion (equation [27]) and the dissipation timescale (equation [23]) leads to the following peculiar situation: in the *stable* region at the lower right of Figure 11, the dissipation time is *shorter* than the collapse timescale, while in the *unstable* region in the upper left of the Figure the dissipation time is *longer* than the collapse timescale. This apparent paradox is resolved when one realizes that stability is determined by the energy content of the cloud and not its energy loss rate.

4.4. Self-Gravitating Forced Runs

A final set of simulations considers stochastically forced runs with self-gravity. These runs are forced in the same manner as the nonself-gravitating, forced runs of §4.2, with the

peak forcing at $k_{\rm pk} = 8\,(2\pi/L)$. The simulations are run without self-gravity for 0.5 sound crossing times, so that the model has a chance to equilibrate; then gravity is turned on.

The standard run, with $\beta = 0.01$, $n_{\rm J} = 4$ (so $E_{G,max} \simeq -25\bar{\rho}Lc_{\rm s}^2$), and forcing power $\delta E/\delta t = 100\bar{\rho}c_s^3$, is shown in Figure 12. The initial 0.5 sound crossing times is identical to the nonself-gravitating runs; collapse occurs as soon as self-gravity is turned on. The longitudinal motions associated with collapse cause a peak in kinetic energy near this time.

Can collapse be prevented in these forced runs? We have performed simulations for a variety of n_J and forcing powers and the results are displayed in Figure 13. The contours in Figure 13 lie at constant $E_G/E_{G,max}$. The pseudo-Jeans analysis leading to equation (27), together with the saturation energy predicted by the fit to the nonself-gravitating, forced runs (equation [19]; the self-gravitating runs have a saturation wave energy that is comparable with this result, but generally smaller by a factor of < 2), predicts that collapse should occur for

$$n_{\rm J} > 0.35\beta^{-0.08}\left(\frac{\dot{E}}{\bar{\rho}c_{\rm s}^3}\right)^{0.33}. \tag{28}$$

The predicted locus of marginal stability for $\beta = 0.01$ is shown as a dashed line in Figure 13. The weak β dependence in equation (28) has been confirmed by runs not shown in the figure. The pseudo-Jeans analysis is thus a fair collapse predictor in this case as well. The corresponding lower limit for the power input needed to prevent collapse is

$$\dot{E} = 24\beta^{0.24}n_{\rm J}^3\bar{\rho}c_{\rm s}^3, \tag{29}$$

which for $\beta = 0.01$ has a coefficient 7.9. In any event, it is clear that transverse magnetic pressure can also prevent collapse in the forced runs.

5. Discussion

5.1. Applications

In this section we translate our results into an astronomical context by applying them to a "typical" molecular cloud. This is a speculative venture, since our simulations employ slab symmetry and make a number of other drastic approximations. The exercise seems worthwhile, however, since the simulations are self-consistent and fully nonlinear, unlike earlier treatments of the problem. Are our results in harmony with the known, observed properties of molecular clouds?

Consider a representative molecular cloud of mean linear dimension $L = 20$pc, number density 100cm^{-3}, kinetic temperature $T = 20$K, and line-of-sight velocity dispersion

Fig. 12.— Time evolution of the magnetic+kinetic, magnetic, and gravitational potential energy in the "standard" run with forcing and gravity. The strength of gravity is such that there are four Jeans lengths inside the simulation scale, and the forcing power is $100\bar{\rho}c_s^3$.

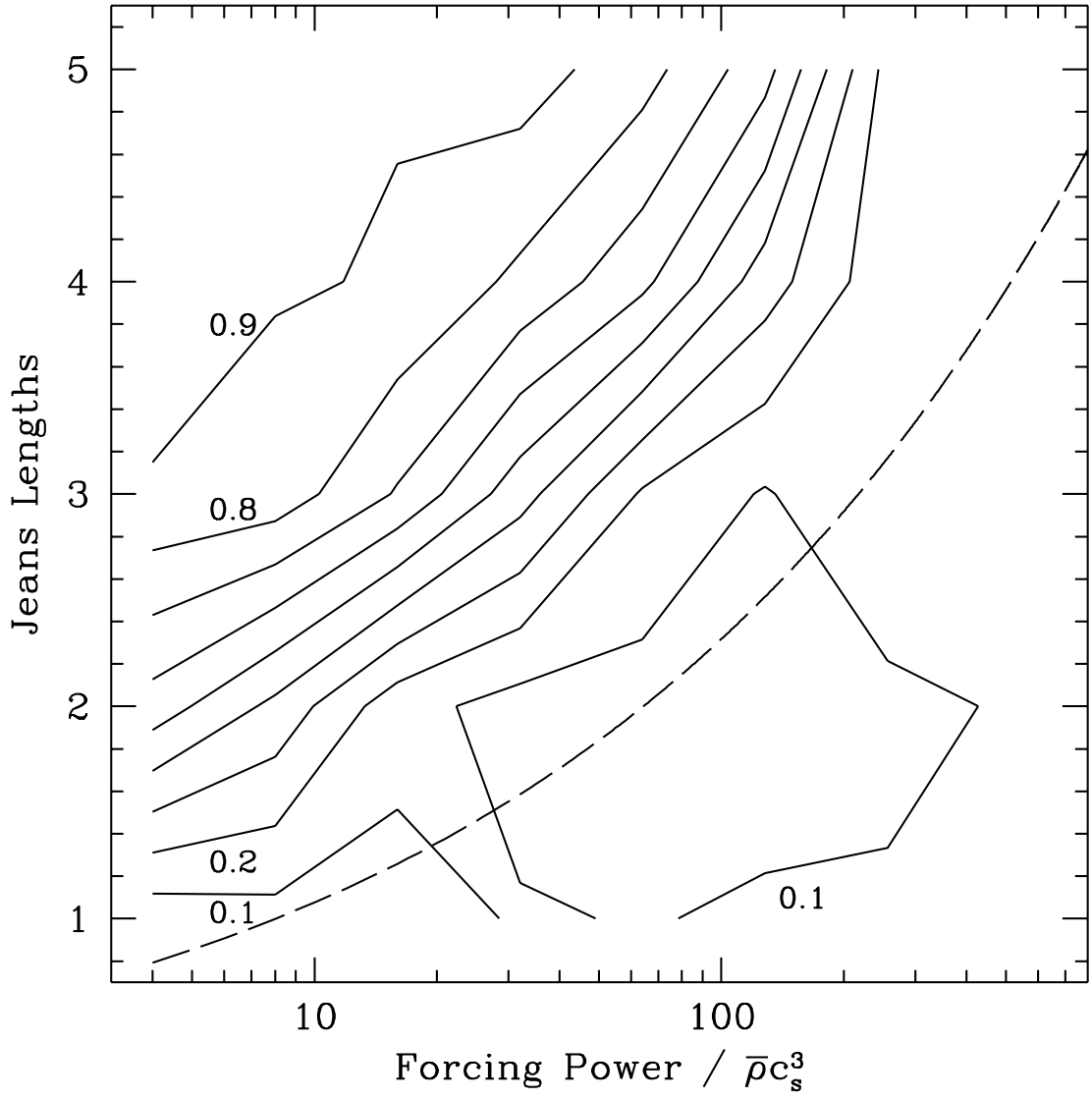

Fig. 13.— A contour plot of the gravitational potential energy $E_{\rm G}$ relative to the maximum gravitational potential energy for a fully-collapsed sheet $E_{\rm G,\,max}$ (eq. [26]) measured at the end of the forced, self-gravitating simulations. $E_{\rm G}/E_{\rm G,\,max}$ is found as a function of the forcing power and Jeans number $n_{\rm J} = L/L_{\rm J}$. The dashed curve shows the locus estimated as the lower limit for collapse in equation (28).

$\sigma_v = 2\mathrm{km\,s^{-1}}$. For mean field strength $B_0 = 20\mu\mathrm{G}$, $\beta = 0.01$. The sound-crossing, gravitational collapse, and Alfvén -crossing timescales for this reference cloud are $t_\mathrm{s} = 74\mathrm{Myr}$, $t_\mathrm{c} = 9.9\mathrm{Myr}$, and $t_\mathrm{A} = 7.6\mathrm{Myr}$ (assuming solar metallicity). The Jeans number $n_\mathrm{J} = L/L_\mathrm{J} = t_\mathrm{s}/t_\mathrm{c} = 7.5$, and the ratio $t_\mathrm{A}/t_\mathrm{c} = 0.76$. Thus, for a static uniform field, the cloud would be unstable parallel and stable perpendicular to the mean field (see §2.2). If the projected area of the cloud is $L^2 = 400\mathrm{pc}^2$, then the kinetic energy per unit surface area is $(3/2)\bar{\rho}\sigma_v^2 L = 87\bar{\rho}Lc_\mathrm{s}^2$. Assuming equipartition between kinetic and perturbed magnetic energy, the wave energy per unit surface area is twice the kinetic energy, $E_W = 173\bar{\rho}Lc_s^2$. Finally, if the cloud's volume is L^3, its total mass is $5.6 \times 10^4\,\mathrm{M}_\odot$.

In the absence of self-gravity or any energy inputs, the cloud would, by assumption, evolve like the free decay simulations of §4.1. In particular, it should evolve similarly to the "standard" decay of Fig. 2, which has $E_W = 100\bar{\rho}Lc_s^2$ and $\beta = 0.01$, and is shown for comparison to the other decays as the central dotted curve in Fig. 5. To provide a more precise comparison, we have run a decay simulation starting from $E_W = 173\bar{\rho}Lc_s^2$. After $9.6\mathrm{Myr}(= 0.16t_\mathrm{s})$, the wave energy would drop by factor ≈ 2, so the velocity dispersion would drop by a factor of $\sqrt{2}$; after 41Myr by a factor ≈ 4, corresponding to a factor of 2 drop in the velocity dispersion. At 15Myr, the cloud contains clumps. Fully 28% of the mass, but only 2% of the volume, lies at densities greater than $10^3\mathrm{cm}^{-3} = 10\bar{\rho}$, while 74% of the volume lies at densities below the mean.

Now suppose the cloud's internal motions are forced (by winds from young stars, for example) at a scale $\lambda = L/8 = 2.5(L/20\mathrm{pc})\mathrm{pc}$, such that the mechanical power input $\mathcal{P}$ equals the wave dissipation rate $\mathcal{L}$ and the observed internal wave energy represents a saturated equilibrium. Again, we temporarily ignore self-gravity. We can use the forced, non-self-gravitating simulations to estimate the required input power and dissipation rate associated with a given equilibrium level of internal kinetic energy. In general the dissipation rate $\mathcal{L}$ should be roughly equal to the luminosity of the cloud in the important gas phase cooling lines, while the mechanical power input $\mathcal{P}$ would equal the sum of energy inputs from young stellar winds (Norman & Silk (1980)), Alfvén waves emerging from collapsing, rotating cloud cores (Gillis, Mestel, & Paris (1979), Gillis, Mestel, & Paris (1979), Mouschovias & Paleologou (1980)), etc. In equilibrium $\mathcal{P} = \mathcal{L}$. Using equations (20) and (22), we find

$$\mathcal{P} = \mathcal{L} = 19 \left(\frac{\sigma_v}{2\mathrm{km\,s^{-1}}}\right)^3 \left(\frac{n_{H_2}}{100\mathrm{cm}^{-3}}\right) \left(\frac{L}{20\mathrm{pc}}\right)^2 \left(\frac{\beta}{0.01}\right)^{1/4} \left(\frac{\lambda}{2.5\mathrm{pc}}\right)^{-1/2} \mathrm{L}_\odot. \qquad (30)$$

A dissipation timescale can be estimated via $t_{diss} = E/\dot{E}$ (eq. 23); the result is

$$t_{diss} = 6.0 \left(\frac{\sigma_v}{3\mathrm{km\,s^{-1}}}\right)^{-1} \left(\frac{L}{20\mathrm{pc}}\right) \left(\frac{\beta}{0.01}\right)^{-1/4} \left(\frac{\lambda}{2.5\mathrm{pc}}\right)^{1/2} \mathrm{Myr}. \qquad (31)$$

This dissipation timescale is comparable to the collapse timescale.

In fact, our reference cloud *is* self-gravitating; it contains $n_J^3 = (7.5)^3 = 410$ Jeans masses. While computational expense prevents us from performing simulations with $n_J \gtrsim 5$, we find that equation (27) is a good predictor of collapse on a dynamical timescale when $n_J \leq 5$. Assuming equation (27) applies for more strongly self-gravitating clouds as well, we find that immediate contraction can be avoided when

$$\langle |\delta \mathbf{B}|^2 \rangle^{1/2} > 18 \left(\frac{L}{20\mathrm{pc}} \right) \left(\frac{n_{H_2}}{100\mathrm{cm}^{-3}} \right) \mu\mathrm{G}, \tag{32}$$

corresponding to

$$\sigma_v > 2.3 \left(\frac{L}{20\mathrm{pc}} \right) \left(\frac{n_{H_2}}{100\mathrm{cm}^{-3}} \right)^{1/2} \mathrm{km\,s}^{-1}. \tag{33}$$

Our reference cloud with $\sigma_v = 2\mathrm{km\,s}^{-1}$ has velocity slightly below the threshold level, and in the absence of energy inputs would contract on a timescale $\sim t_\mathrm{c}$.

The reference cloud could be supported in an indefinite equilibrium if it were supplied with energy at a scale λ, as in the forced, self-gravitating simulations. Using equations (29) and (22), we find that an input power of

$$\mathcal{P} = 27 \left(\frac{L}{20\mathrm{pc}} \right)^5 \left(\frac{n_{H_2}}{100\mathrm{cm}^{-3}} \right)^{5/2} \left(\frac{\beta}{0.01} \right)^{1/4} \left(\frac{\lambda}{2.5\mathrm{pc}} \right)^{-1/2} \mathrm{L}_\odot \tag{34}$$

or greater is required to support the cloud in a true equilibrium. A smaller supply of power would lead to gradual contraction. Notice that the power required to support the current level of turbulent energy in our reference cloud (eq. 30) would be insufficient to support it indefinitely against gravity. For the latter, the higher power level of equation (34) would be required, and the one-dimensional velocity dispersion would be raised to the level indicated in equation (33).

The "reference" cloud described above is meant to represent a cloud like Orion A (Bally et al (1987)) or the Rosette nebula (Williams, Blitz, & Stark (1995)). For clouds as large as this, we have had to extrapolate our fits to larger values of the Jeans number and input power than we were able to compute directly. On the other hand, smaller self-gravitating clouds such as Taurus-Auriga (Cernicharo (1991)) or Ophiuchus (Loren (1989a), Loren (1989b)) are within the parameter range we have simulated, and therefore the results presented in the figures of §4 can be used directly. Diffuse, high-latitude clouds may be best represented by our unforced, non-self-gravitating simulations.

The power requirements for sustaining turbulence and counteracting gravity of equations (30) and (34) are reasonable for GMCs. For example, the total hydrodynamic

outflow momentum observed in Orion A (which has properties comparable to our reference cloud) is estimated at $320\,\mathrm{M}_\odot\mathrm{km\,s}^{-1}$ (Fukui et al (1993)), which for mean outflow velocity $30\mathrm{km\,s}^{-1}$ and outflow lobe size 0.75pc (cf. Fukui et al (1989)) implies a characteristic power input of $33\,\mathrm{L}_\odot$. Thus our results are in accord with observations.

Finally, let us suppose that clouds evolve in quasi-equilibrium, and support can ultimately be ascribed to the power originating in young stellar outflows. Then by equating the required power $\mathcal{P}$ to the total wind mechanical luminosity $G\dot{\mathcal{M}}_* M_*/R_c$ we can obtain a total star formation rate $\dot{\mathcal{M}}$ in the cloud. Here we absorb the details of the wind acceleration mechanism into the characteristic radius R_c where the wind originates (see, e.g., Shu et al (1994)), and the uncertainties associated with the coupling of the wind to the rest of the cloud into the scale λ. Scaling R_c to 0.1 AU and using equation (34), we find

$$\dot{\mathcal{M}}_* = 2{\times}10^{-5} \left(\frac{L}{20\mathrm{pc}}\right)^5 \left(\frac{n_{H_2}}{100\mathrm{cm}^{-3}}\right)^{5/2} \left(\frac{\beta}{0.01}\right)^{1/4} \left(\frac{\lambda}{2.5\mathrm{pc}}\right)^{-1/2} \left(\frac{R_c}{0.1\,\mathrm{AU}}\right) \left(\frac{M_*}{\mathrm{M}_\odot}\right)^{-1} \mathrm{M}_\odot\mathrm{yr}^{-1}. \tag{35}$$

This implies a star formation timescale $M(cloud)/\dot{\mathcal{M}}_* \simeq 3 \times 10^9\mathrm{yr}$, which is about 300 times the dynamical collapse time. It also implies that over a cloud lifetime of perhaps $3 \times 10^7\mathrm{yr}$ the cloud will turn about 1% of its mass into stars.

5.2. Perspective

It behooves us to remind the reader of some of the shortcomings of our treatment. The most severe is the use of slab (one dimensional) symmetry. In higher dimensions, dissipation rates may rise because new, transverse decay modes will be available. On the other hand, dissipation rates could fall somewhat because clumps, once formed, need not collide with each other, as they do in one dimension. Fortunately, an extension to two dimensions is immediately practicable.

Although the use of slab symmetry is likely the leading source of error in our calculation, we have made other approximations that contribute as well, and that could be relaxed in future treatments of this problem. In this work, we have used an isothermal equation of state. Numerical work has shown, however, that realistic molecular cooling can have a significant effect on fragmentation during gravitational collapse (e.g. Monaghan & Lattanzio (1991)). We also neglect ambipolar diffusion. This is likely to have particularly significant effects at small scales in clouds, where MHD waves cannot propagate. Even for Alfvén waves on the scale of the GMCs, the ambipolar-diffusion damping timescale can be smaller than the dynamical timescale if the only source of ionization is cosmic rays at a rate $10^{-17}s^{-1}$. Overall, inclusion of ambipolar diffusion would tend to increase total dissipation

rates, and to steepen the power spectrum.

Another idealization in our simulations is the periodic boundary conditions. These boundaries prevent any wave energy losses from our model clouds by radiation to an external medium, as would reflecting boundary conditions. Estimates indicate that under certain conditions wave radiation may dominate other energy losses from molecular clouds (cf. Elmegreen (1985)). For a linear amplitude wavetrain, the transmission coefficient at the cloud edge is small when the density changes sharply over a distance smaller than the wavelength. Since most of the energy in our simulations is at the largest scales, our results could be sensibly applied to clouds with edge gradients sharper than the inverse of the cloud size.

Finally, we have neglected cosmic ray pressure and transport, radiative transfer effects, and, of course, feedback from star formation. It is not likely that these effects can be incorporated in any realistic way in the near future. Our forcing algorithm does model power input by, e.g., stellar winds, but only in a crude fashion.

Nevertheless, our treatment does represent significant progress. As far as we are aware, it is the first fully self-consistent treatment of a turbulent, magnetically dominated, compressible, self-gravitating fluid. Our self-consistent simulations with realistic field strengths and velocities lead to a highly inhomogeneous state characterized by MHD discontinuities. This state bears little resemblance to any regime that has been well studied in the past. In particular, while some results carry over from quasi-linear theories and theories of incompressible, eddy-dominated turbulence, neither can adequately represent the internal dynamics of molecular clouds.

5.3. Summary

In this paper, we set out to explore the hypothesis that magnetic forces are crucial to the internal dynamics of Galactic molecular clouds. We were motivated by the proposal that the fluctuating velocity field in MHD waves is responsible for the observed hypersonic turbulence in molecular clouds, while the associated magnetic field fluctuations provide a pressure vital in supporting clouds against gravitational collapse and confining non-self-gravitating clumps. In particular, we were interested in whether observed molecular clouds represent dynamical equilibria, and more generally what is required to sustain a given level of MHD turbulence in the face of nonlinear dissipation and self-gravity. A quasistatic equilibrium is possible even with wave decay; cloud turbulence may be replenished for example by the gravitational potential energy liberated from rotating cloud cores and disks

when they collapse and accrete to form stars.

This work uses numerical simulations to investigate large-amplitude ($\delta v/v_{\rm A} \sim 1$) MHD turbulence under density, temperature, and magnetic field conditions appropriate for Galactic molecular clouds. Computational expense has imposed some sacrifices of realism in this first self-consistent treatment of turbulence in a highly compressible, magnetically-dominated ($c_{\rm s}/v_{\rm A} \ll 1$) fluid. Our main idealizations are to restrict the dynamics to plane-parallel geometry with periodic boundary conditions, and to ignore ion-neutral slippage. This is the simplest possible model that incorporates magnetic fields and gravity self-consistently.

We have performed four types of numerical simulations. In the first (§4.1), we evolved a spectrum of large-amplitude Alfvén -wave turbulence to determine the free decay rate. In these simulations, we also investigated the spectral evolution of the turbulence and formation of density structure. In our second set of simulations (§4.2), we set out to evaluate the level of internal stochastic forcing (intended to model power inputs like young stellar winds) required to sustain a given level of turbulent kinetic energy. In our third set of simulations (§4.3), we included self-gravity in model clouds initiated with differing levels of wave energy to establish collapse thresholds while allowing for turbulent decay. In our final set of simulations (§4.4), we applied stochastic internal forcing to self-gravitating clouds to evaluate the power input needed to prevent collapse. As a template for using the dimensionless results of §4, we translate into physical units for a "reference" cloud in §5.1.

Our major conclusions are as follows: (1) We have confirmed that nonlinear disturbances in ideal MHD can support a model cloud against gravitational collapse, provided that the perturbed magnetic energy is maintained at a level exceeding the binding energy of the cloud (cf. eq.[32]). Gravity is opposed by a gradient in the time-varying magnetic pressure due to the components of the field perpendicular to the mean field. (2) We have characterized the dynamical state of highly nonlinear, $c_s^2/v_{\rm A}^2 \ll 1$ MHD systems. Such systems contain strong density contrasts, with much of the volume effectively evacuated and most of the mass concentrated into small regions. High density "clumps" form and disperse over time, with a secular trend toward increasingly large concentrations and coherent motions as energy cascades to larger scales. These nonlinear, magnetically dominated systems contain numerous MHD discontinuities, which naturally give rise to a wave energy power spectrum approximately $|B_{\perp,k}|^2 \propto |v_{\perp,k}|^2 \propto k^{-s}$ with $s \sim 2$, or linewidth-size relation approximately $\sigma_v(R) \propto R^{1/2}$. The shape of the power spectra at late times are essentially independent of the initial input spectrum or energy injection scale. (3) We have calculated a decay rate for nonlinear MHD waves in slab symmetry by equating forcing and dissipation rates in a saturated equilibrium. The dissipation time,

given in physical units in equation (31), is longer than some naive estimates. In particular, when the cloud is stirred at scales comparable to its size, the dissipation time exceeds the "eddy turnover time" L/σ_v by $(v_{\rm A}/c_{\rm s})^{1/2}$ times an order-unity factor, and the Alfvén -wave crossing time by an additional factor $v_{\rm A}/\sigma_v$ (see eq.[23]). Peak dissipation rates for free decay obey approximately the same scaling in σ_v, $v_{\rm A}$, and $c_{\rm s}$ as the dissipation rate in saturated equilibrium. Because of the present restricted geometry and negligible friction, our computed dissipation rates are likely lower limits.

We are especially grateful to Jim Stone for helping to initiate this project. We would also like to thank Bruce Elmegreen, Chris McKee, Phil Myers, and Phil Solomon, for interesting discussions, Alyssa Goodman, Jeremy Goodman, and Jerry Ostriker for comments on a draft of this paper, and the referee Ellen Zweibel for a discerning review. This work was supported in part by NASA grant NAG 52837.

REFERENCES

Arons, J. & Max, C. E. 1975, ApJ, 196, L77

Bally, J., Langer, W. D., Stark, A. A., & Wilson, R. W. 1987, ApJ, 312, L45

Bertoldi, F. & McKee, C. F. 1992, ApJ, 395, 140

Black, J. H. 1987, in Interstellar Processes, ed. D. J. Hollenbach & H. A. Thronson (Dordrecht: Reidel), p. 731

Blitz, L., & Shu, F. H. 1980, ApJ, 238, 148

Blitz, L. 1993, in Protostars and Planets III, ed. E. Levy & J. Lunine (Tucson: University of Arizona Press), p. 125

Burlaga, L. F., & Mish, W. H. 1987, J. Geophys. Res., 92, 1261

Carr, J. S. 1987, ApJ, 323, 170

Caselli, P., & Myers, P. C. 1995, ApJ, 446, 665

Chandrasekhar, S. & Fermi, E. 1953, ApJ, 118, 116

Cernicharo, J. 1991, in The Physics of Star Formation and Early Stellar Evolution, Eds. C. J. Lada & N. D. Kylafis (Dordrecht: Kluwer), p. 287

Clifford, P., & Elmegreen, B. G. 1983, MNRAS, 202, 629

Cohen, R. H., & Kulsrud, R. M. 1974, Phys. Fluids 17, 2215

Cox, J. P. 1980, Theory of Stellar Pulsation (Princeton: Princeton University Press)

Crutcher, R. M., Troland, T. H., Goodman, A. A., Heiles, C., Kazes, I., & Myers, P. C., ApJ, 407, 175

Dame, T. M., Elmegreen, B. G., Cohen, R. S., & Thaddeus, P. 1986, ApJ, 305, 892

Davidson, J. A., Schleuning, D., Dotson, J. L., Dowell, C. D., & Hildebrand, R. H. 1995, in Astronomical Society of the Pacific, Airborne Astronomy Symposium on the Galactic Ecosystem: From Gas to Stars to Dust, Volume 73, p 225

Dewar, R. L. 1970, Phys. Fluids 13, 2710

Dotson, J. 1996, submitted to the ApJ

Elmegreen, B. G. 1985, ApJ, 299, 196

Elmegreen, B. G. 1990, ApJ, 361, L77

Elmegreen B. G. 1991, in The Physics of Star Formation and Early Stellar Evolution, Eds. C. J. Lada & N. D. Kylafis (Dordrecht: Kluwer), p. 35

Elmegreen B. G. 1993, in Protostars and Planets III, Eds. E. H. Levy & J. I. Lunine (Tucson: Univ. of Arizona Press), p. 97

Falgarone, E. & Puget, J. L. 1986, A&A, 162, 235

Falgarone, E., & Phillips, T. G. 1990, ApJ, 359, 344

Falgarone, E., Phillips, T. G., & Walker, C. K. 1990, ApJ, 378, 186

Falgarone, E. & Pérault, M. 1987, in Physical Processes in Interstellar Clouds, eds. G. E. Morfill & M. Scholer (Dordrecht: Kluwer), p. 59

Falgarone, E., Puget, J. L., & Pérault, M. 1992, A&A, 257, 715

Fatuzzo, M., & Adams, F. C. 1993, ApJ, 412, 146

Fukui, Y., Iwata, T., Takaba, H., Mizuno, A., Ogawa, H., Kawabata, K., & Sugitami, K. 1989, Nature, 342, 161

Fukui, Y., Iwata, T., Mizuno, A., Bally, J., & Lane, A. P. 1993, in Protostars and Planets III, ed. E. Levy & J. Lunine (Tucson: Univ. of Arizona Press), p. 603

Fuller, G. A., & Myers, P. C. 1992, ApJ, 384, 523

Gillis, J., Mestel, L., & Paris, R. B. 1979a, MNRAS, 187, 311

Gillis, J., Mestel, L., & Paris, R. B. 1979a, MNRAS, 187, 337

Ghosh, S., & Goldstein, M.L. 1994, JGR, 99, 13351

Goldreich, P., & Sridhar, S. 1995, ApJ, 438, 763

Goldstein, M.L. 1978, ApJ, 219, 700

Goodman, A. A., & Heiles, C. 1994, ApJ, 424, 208

Heiles, C., Goodman, A. A., McKee, C. F., & Zweibel, E. G. 1993, in Protostars and Planets III, ed. E. Levy & J. Lunine (Tucson: University of Arizona Press), p. 279

Herbertz, R., Ungerechts, H., & Winnewisser, G. 1991, A&A, 249, 483

Hildebrand, R. H., Dotson, J. L., Dowell, C. D., Platt, S. R., Schleuning, D., Davidson, J. A., & Novak, G. 1995, in Astronomical Society of the Pacific, Airborne Astronomy Symposium on the Galactic Ecosystem: From Gas to Stars to Dust, Volume 73, p 97

Kulsrud, R. M., & Pearce, W. P. 1969, ApJ, 156, 445

Larson, R. B. 1981, MNRAS, 194, 809

Loren, R. B. 1989, ApJ, 338, 902

Loren, R. B. 1989, ApJ, 338, 925

McKee, C. F. 1989, ApJ, 345, 782

McKee, C. F. & Zweibel, E. G. 1995, ApJ, 440, 686

McKee, C. F., Zweibel, E. G., Goodman, A. A., & Heiles, C. 1993, in Protostars and Planets III, ed. E. Levy & J. Lunine (Tucson: University of Arizona Press), p. 327

Mestel, L., & Spitzer, L. 1956, MNRAS, 116, 503

Miesch, M. S., & Scalo, J. M. 1995, ApJ, 450, L27

Monaghan, J. J., & Lattanzio, J. C. 1991, ApJ, 375, 177

Moneti, A., Pipher, J. L., Helfer, H. L., McMillan, R. S., & Perry, M. L., ApJ, 282, 508

Mouschovias, T. 1976, ApJ, 207, 141

Mouschovias, T. C., & Paleologou, E. V. 1980, Moon & Planets, 22, 31

Mouschovias, T., & Spitzer, L. 1976, ApJ, 210, 326

Mouschovias, T., in The Physics of Star Formation and Early Stellar Evolution, Eds. C. J. Lada & N. D. Kylafis (Dordrecht: Kluwer), p. 61

Myers, P. C., & Goodman, A. A. 1988a, ApJ, 326, L27

Myers, P. C., & Goodman, A. A. 1988b, ApJ, 329, 392

Myers, P. C. & Khersonsky, V. K. 1995, ApJ, 442, 186

Nakano, T. 1984, Fund. Cosmic Phys. 9, 139

Norman, C., & Silk, J. 1980, ApJ, 238, 158

Passot, T., Pouquet, A., & Woodward, P. 1988, A&A, 197, 228

Pérault, M., Falgarone, E., & Puget J. L. 1985, A&A, 152, 371

Porter, D., Pouquet, A., & Woodward P. 1992, Theor. Comp. Flu. Dyn., 4, 13

Pudritz, R. E., ApJ, 350, 195

Ryu, D., & Jones, T.W. 1995, ApJ, 442, 228

Sagdeev, R. Z., & Galeev, A. A. 1969, Nonlinear Plasma Theory (New York: W. A. Benjamin)

Scalo, J. M., & Pumphrey, W. A. 1982, ApJ, L29

Shu, F. H. 1992, The Physics of Astrophysics, vol. 2 (Mill Valley: University Science Books)

Shu, F.H., Adams, F.C. & Lizano, S. 1987, ARA&A, 25, 23

Shu, F., Najita, J., Ostriker, E., Wilkin, F., Ruden, S., & Lizano, S. 1994, ApJ, 429, 781

Solomon, P. M., Rivolo, A. R., Barrett, J., & Yahil, A. 1987, ApJ, 319, 730

Spitzer, L. 1942, ApJ, 95, 329

Spitzer, L. 1968, in Nebulae and Interstellar Matter, ed. B. M. Middlehurst & L. H. Aller (Chicago: Univ. of Chicago Press), p. 1

Sridhar, S., & Goldreich, P. 1994, ApJ, 432, 612

Stone, J. M. & Norman, M. L. 1992a, ApJSupp, 80, 753

Stone, J. M. & Norman, M. L. 1992b, ApJSupp, 80, 791

Tomisaka, K., Ikeuchi, S., & Nakamura, T. 1988, ApJ, 335, 239

Williams, J. P., Blitz, L. & Stark, A. A. 1995, ApJ, 451, 252

Zweibel, E. G., & Josafatsson, K. 1983, ApJ, 270, 511

Zweibel, E. & McKee, C. F. 1995, ApJ, 439, 779